ELSEVIER

Journal of Structural Geology 28 (2006) 1588–1606

JOURNAL OF STRUCTURAL GEOLOGY

www.elsevier.com/locate/jsg

Sheath folds as discriminators of bulk strain type

G.I. Alsop [a,*], R.E. Holdsworth [b]

[a] Crustal Geodynamics Group, School of Geography & Geosciences, University of St. Andrews, Fife KY16 9AL, UK
[b] Reactivation Research Group, Department of Earth Sciences, University of Durham, Durham DH1 3LE, UK

Received 6 February 2006; received in revised form 8 May 2006; accepted 16 May 2006
Available online 7 August 2006

Abstract

Nested elliptical closures defining ''eye-folds'' represent classic (y–z) cross sections through highly curvilinear sheath folds generated during intense ductile deformation in metamorphic rocks. Systematic analysis of 1425 such eye-folds based on our own field observations and examples from the published literature reveals distinct and consistent differences in ellipticites measured from the outer- (R_{yz}) to the inner-most ($R_{y'z'}$) elliptical ''rings'' of individual sheaths. The variation in overall aspect ratios from outer to inner rings is defined as R' (where $R' = R_{yz}/R_{y'z'}$) and may display a relative increase or decrease in ellipticity to define '*cats-eye*' ($R' < 1$) or '*bulls-eye*' ($R' > 1$) fold patterns respectively. Layer thicknesses may also be measured along the y axis (parallel to the axial surface) (t_y) and at 90° to this along the z axis (t_z) to define the ratio of T_{yz}. Sheath folds generated during broadly simple shear deformation ($k \cong 1$) display (mean) R_{yz} 4.61, T_{yz} 3.31 and cats-eye-folds (R' 0.69). Sheath folds generated during general shear also display cats-eye-folds with identical mean R' 0.69 values, but greater thickness variations and elliptical ratios (T_{yz} 4.35, R_{yz} 5.76). Thus, within both simple- and general shear-dominated deformations, the overall variation in layer thickness (T_{yz}) and ellipticity of eye-folds (R_{yz}) increases with increasing deformation and a greater component of pure shear, whilst the R' value remains constant and reflects original fold patterns. Sheath folds formed during constrictional ($k > 1$) deformation display markedly lower aspect ratios (R_{yz} 2.42) and thickness variations (T_{yz} 2.94), together with distinctive bulls-eye-folds (R' 1.23). These empirical relationships suggest fundamental and universal constraints on curvilinear fold generation across this broad spectrum of deformation types, and allow sheath folds to act as both effective (>95% consistent) and robust discriminators of bulk strain type.
© 2006 Elsevier Ltd. All rights reserved.

Keywords: Sheath folds; Shear zones; Strain; Ductile deformation; Eye-folds

1. Introduction

The development in high-strain zones of curvilinear folds was recognised in the 1960s (e.g. Voll, 1960; Carey, 1962; Nicholson, 1963; Dalziel and Bailey, 1968; Dearman, 1969) although the descriptive term sheath fold was only more recently introduced into the literature (Carreras et al., 1977; Quinquis et al., 1978; Minigh, 1979). Sheath folds may most simply be defined as folds in which the hinge-line displays >90° of curvature when traced along its length (Ramsay and Huber, 1987), and are now typically considered to reflect progressive and intense deformation (see Alsop and Holdsworth, 2004a,b). Most sheath folds are classically thought to form by the sequential rotation of fold hinges that initiate at high angles to shear during progressive non-coaxial deformation (Cobbold and Quinquis, 1980). Gentle curvilinearity of the initial fold hinge is therefore accentuated during subsequent shearing to create highly curvilinear sheath folds (e.g. Cobbold and Quinquis, 1980; Ramsay, 1980).

Sheath folds can be described as containing an x axis along the length of the tube or tongue, whilst cross sections normal to the x axis display elliptical geometries defining the intermediate (y) and short (z) axes (Fig. 1). Such elliptical sections or nested rings define eye-folds (also known as ''eye-structures'' or ''closed folds'' (Ramsay, 1962; Nicholson, 1963; Mukhopadhyay and

* Corresponding author.
E-mail addresses: gia@st-andrews.ac.uk (G.I. Alsop), R.E.Holdsworth@durham.ac.uk (R.E. Holdsworth).

0191-8141/$ - see front matter © 2006 Elsevier Ltd. All rights reserved.
doi:10.1016/j.jsg.2006.05.005

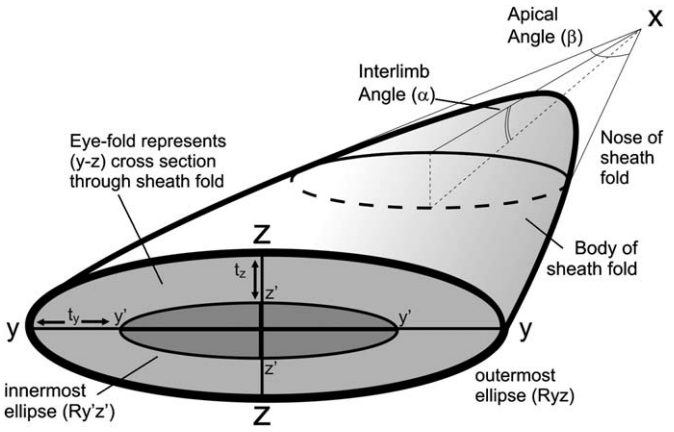

Fig. 1. Schematic sketch illustrating the x, y and z axes of a sheath fold together with the inter-limb angle (α) and apical angle (β) of the curvilinear fold hinge-line. Y–Z orientated cross sections across the sheath fold result in eye-fold geometries. Elliptical ratios of the outer-most ring (R_{yz}) and inner-most ring ($R_{y'z'}$) are also given. The thickness of any individual layer may be measured along the y axis (t_y) and at 90° to this along the z axis (t_z) to provide a ratio (T_{yz}) of layer thickening/thinning. See text for discussion.

Sengupta, 1979). Thus, eye-folds are classically considered to represent two dimensional (y–z) cross sections cutting directly across the length (x) of the sheath fold (Fig. 1). It has long been recognised that these eye-folds defined by layering may display y–z aspect ratios (R_{yz}) that vary between circular (1:1) and highly elliptical (1:25) (Williams and Zwart, 1977). Larger R_{yz} aspect ratios become increasingly difficult to identify owing to attenuation and transposition of fold limbs, and the present study is therefore largely based on analyses of sheath folds displaying $R_{yz} < 20$.

The x, y and z geometric axes of sheath folds are generally considered to lie sub-parallel with the X, Y and Z axes of the finite strain ellipsoid (e.g. Quinquis et al., 1978; Minigh, 1979). The x axis of the sheath fold is thus broadly parallel to the mineral elongation lineation (X), which marks the transport direction during intense non-coaxial deformation, whilst the sheath y axis lies on the plane of the foliation (X–Y surface) with the z axis forming the normal to that plane. Mineral lineations defining the X-direction and associated with the development of sheath folds may also be marked by an anisotropy of magnetic susceptibility (AMS) fabric that aids further in the interpretation of structural relationships (e.g. Lefort et al., 2001).

Despite the increasing recognition that shear zones may display a variety of strain types that deviate significantly from simple shear (e.g. Alsop and Holdsworth, 2004c and references therein), the concept of sheath generation is still very much based on progressive deformation marked by simple shear (e.g. Cobbold and Quinquis, 1980). In order to investigate and test the role of different strain types on the geometry and evolution of sheath folds, we have drawn on data from a wide range of deformation zones marked by simple shear, and general shear in which a pure shear component has also operated. Sheaths from settings that may deviate significantly from plane strain ($k = 1$) deformation such as constrictional shear zones have also been analysed for comparison. Our analyses of natural sheath folds are based on our own observations and data, together with an extensive review of the sheath fold literature published largely during the past 40 years. This investigation suggests that highly curvilinear folds and sheath folds are far more common than previously realised with 1425 elliptical sections being analysed from a sample of 501 individual sheath folds in this study.

Recent debate has centred on whether the shape of sheath folds and associated eye-folds may reflect variable strain intensity associated with non-coaxial deformation (e.g. Goscombe, 1991, p. 314). In addition, it has been claimed (Ez, 2000) that most sheath folds do not display a great enough variation in the thickness of layering to be generated by simple shear alone, and that a constrictional component of deformation may be more appropriate in such cases. Despite these general associations and inferences, this study represents the first to analyse natural examples of sheath fold geometries generated during broadly simple shear, general shear (where an additional component of pure shear has operated with simple shear) and constrictional deformation. The aim of this work is therefore to record and compare sheath geometries developed within these different tectonic settings by establishing a new descriptive framework based on easily recorded parameters. This may allow sheath folds to act as effective discriminators of strain type.

In the present paper, we restrict our analysis to sheath folds developed during intense ductile deformation within metamorphic rocks, but it is important to note that such structures are also known to develop during intense deformation in a wide variety of other geological settings, e.g. slumps, sub-glacial deformation, flow of salt and magmas.

2. A new framework for describing eye-folds

Although eye-folds marked by closed elliptical patterns have obviously long been recognised and recorded (e.g. Dale, 1921), no rigorous framework exists for the detailed analysis of such folds. The elliptical ratio (R_{yz}) of any sheath fold will obviously vary as a consequence of the length of the intermediate (y) axis, which is controlled by the degree of hinge-line curvature (the apical angle, β), coupled with the dimension of the short (z) axis which reflects the interlimb angle (α) (Fig. 1). The short (z) axis of the ellipse thus marks the direction of greatest curvature, while the intermediate (y) axis reflects the direction of least curvature for any given curvi-planar surface (see Lisle, 2003). These R_{yz} elliptical cross sections are normal to the long (x) axis of the sheath fold, which is typically more difficult to measure in most natural exposures. The thickness of any individual layer may be measured along the y axis within the axial (x–y) surface of the sheath fold (t_y), and at 90° to this along the z axis (t_z) (Fig. 1). The ratio T_{yz} (where $T_{yz} = t_y/t_z$) will therefore reflect the relative thickening or thinning of layers from the limbs to the hinge of the sheath fold.

Mies (1993, p. 989) suggests that y–z sections of sheath folds should be measured at the mid-point of the length (x) of the sheath. However, in practice, this theoretical measurement is impossible to achieve without complete excavation

of exposures to extract 3-D sheath surfaces. However, the results presented below suggest that as long as sectioning avoids the nose and base of the outer-fold, and lies orthogonal to the x axis of the sheath, then reliable and consistent results are obtained. This view is supported by our analysis of sheath folds in three dimensions, together with the serial sectioning of sheaths by several authors (e.g. Minigh, 1979; Faure, 1985; Crispini and Capponi, 1997).

Intermediate (y) and short (z) axes of sheath folds have been measured directly in the field, and have also been calculated from a variety of additional data sources including photographs, maps and plans representing cross sections through sheath folds. These y–z sections are normal to the long axis (x) of the sheath, with simple trigonometric calculations being made to correct for plunging hinges and inclined axial surfaces where necessary. Closed dome and basin forms generated by clear refolding associated with Type 1 interference patterns (Ramsay, 1962) and fabric overprinting are deliberately excluded from the data set used in this study.

As noted above, y–z cross sections through sheath folds are characterised by ''nested'' elliptical rings, which represent a series of surfaces defining sheath geometries positioned one within another. Although such eye-folds have long been recognised (e.g. Nicholson, 1963), it is still unclear how (a) the shape and elliptical ratio (R_{yz}) of eye-folds may vary and (b) how the inner parts of the sheath fold eye may vary in relation to the outer-most surfaces. Analysis of these variations may provide further insights into the mechanisms of deformation and folding.

In order to systematically investigate the geometry of individual sheath folds, the y and z axes forming the outer- (R_{yz}) and inner-most ($R_{y'z'}$) elliptical ''rings'' which define the overall eye-fold are measured in a plane normal to the length (x) of the sheath. Total variation in the outer to inner elliptical ratio (R') of individual sheaths may then be established by calculating $R_{yz}/R_{y'z'}$. Inner and outer ellipses of sheath folds can on this basis be divided into three major categories or classes described below.

2.1. Type A or ''analogous-eye-folds''

Type A or analogous-eye-folds are defined as where the cross sectional ellipticity of the inner-most ring ($R_{y'z'}$) is equivalent to that of the outer-most ring ($R_{y'z'} = R_{yz}$) such that overall ellipticity remains constant. This results in concentric and self similar elliptical rings which are directly analogous to one another with $R' = 1$ (Fig. 2a).

Sheath folds displaying Type A or analogous-eye-folds have been frequently recorded in the literature (e.g. Nicholson, 1963; Hansen, 1971; Lacassin and Mattauer, 1985; Malavieille, 1987b; Skjernaa, 1989; Goscombe, 1991; Fletcher and Bartley, 1994) and we have also undertaken our own detailed analysis and mapping of such eye-folds (Figs. 2ai, aii, 3, and 4). All of our sections are based on maps of the y–z section surface that is normal to the mineral lineation marking the x-direction of the sheath fold. Analysis of our case studies reveals broadly analogous-eye-folds (R' 0.92) associated with only moderate elliptical ratios (R_{yz} 3.84) and variations in layer thickness (T_{yz} 2.8) (Fig. 2a). The studied folds also display hinge apical angles (β) of $\sim 40^\circ$ associated with tight inter-limb angles (α) of $<30^\circ$.

Sheath folds displaying Type A analogous-eye-folds ($R' = 1$) may intuitively be thought to represent the dominant type of fold, with the geometry of outer layers controlling and pre-determining that of the inner eye. Indeed, based on observations in Sweden, Skjernaa (1989, p. 697) suggests that there is no general trend in the variation of elliptical ratios from outer to inner layers of sheath folds. Mies (1993, p. 986) notes that ''similarly proportioned and similarly orientated elliptical patterns occur in cross section, one nested inside the other''. However, our extensive analysis of nested elliptical closures frequently reveals distinct and consistent differences between the outer- (R_{yz}) and inner-most ($R_{y'z'}$) elliptical ''rings'' defining the overall eye-fold, with most cross sections through sheath folds displaying marked variations in the outer to inner elliptical ratios ($R' \neq 1$) which are described below.

2.2. Type B or ''bulls-eye-folds''

Type B or bulls-eye-folds are defined as where the cross sectional ellipticity of the inner-most ring ($R_{y'z'}$) is less than that of the outer-most ring ($R_{y'z'} < R_{yz}$) such that overall ellipticity decreases towards the centre. This results in increasingly circular rings or ''pupils'' in the centre of the ''bulls-eye'' with $R' > 1$ (Fig. 2b).

Numerous examples of sheath folds displaying Type B or bulls-eye-folds ($R' > 1$) are found in the literature (e.g. Nicholson, 1963; Nicholson and Walton, 1963; Hansen, 1971; Mattauer et al., 1981; Kelly et al., 2000; Terry and Robinson, 2003) and we have also undertaken detailed mapping of such eye-folds (Figs. 2bi, bii, 5). Analysis of these case studies reveals distinct bulls-eye-folds (R' 1.11) associated with low elliptical ratios (R_{yz} 2.25) and only limited variation in layer thickness (T_{yz} 2.25) (Fig. 2b). A pronounced mineral lineation (which may intensify into a rodding structure) bisects the sheath folds and associated eye-folds and is typically parallel to an intersection lineation. The studied folds notably display extremely tight inter-limb (α) and hinge apical angles (β) of $<5^\circ$ which also accentuates the linear character of the rocks.

2.3. Type C or ''cats-eye-folds''

Type C or cats-eye-folds are defined as where the cross sectional ellipticity of the inner-most ring ($R_{y'z'}$) is greater than that of the outer-most ring ($R_{y'z'} > R_{yz}$) such that overall ellipticity increases towards the centre. This results in pronounced elliptical rings in the centre of the ''cats-eye'' with $R' < 1$ (Fig. 2c).

Sheath folds displaying Type C or cats-eye-folds ($R' < 1$) are the most common type recorded within the literature (e.g. Quinquis et al., 1978; Minigh, 1979; Faure, 1985; Boyle, 1987; White and Flagler, 1992; Alsop, 1994; Harms et al., 2004). Analysis of our case studies reveals distinct cats-eye-folds (R' 0.64) associated with pronounced elliptical ratios (R_{yz}

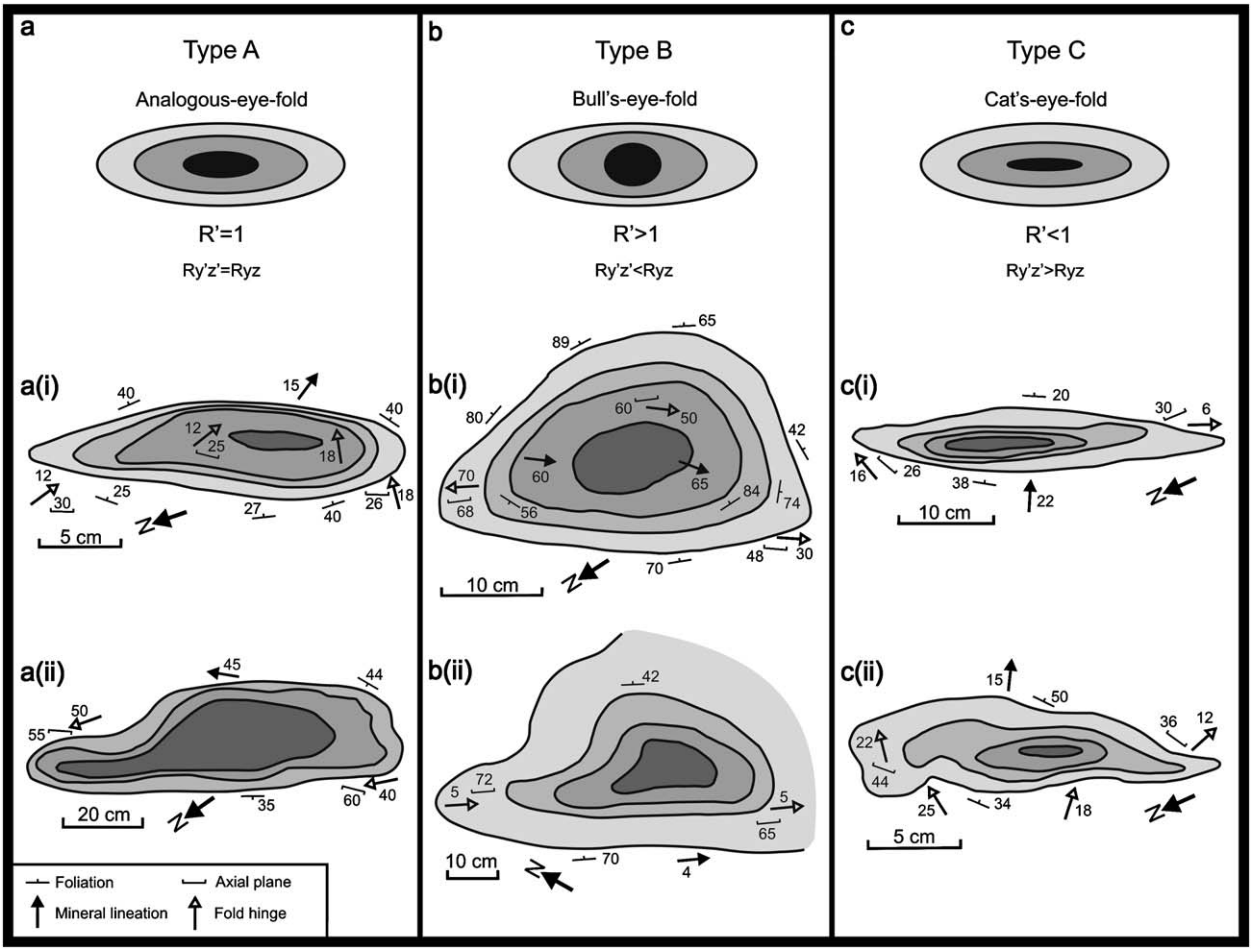

Fig. 2. Schematic diagram illustrating the variation in elliptical ratios (R') within (a) Type A, Analogous-eye-fold, (b) Type B, Bulls-eye-fold and (c) Type C, Cats-eye-fold. Down-plunge maps illustrate $y-z$ cross sections through each type of eye-fold pattern from Moine and Lewisian rocks in NW Scotland. All coordinates refer to the UK National Grid. (ai) Map of analogous-eye-fold in a gentle-moderately inclined sheath fold developed in Moine psammites, Sleiteil (NC6268962929). The individual layers show a moderate variation in thickness (T_{yz} 3.13) whilst the elliptical ratio (R_{yz} 3.0) remains identical from the outer rings towards the centre of the closure ($R' = 1$). (aii) Map of broadly analogous-eye-fold developed in Moine psammites at Loch Quoich (NH0147604056). The individual layers show a moderate variation in thickness (T_{yz} 2.4) whilst the elliptical ratio (R_{yz} 4.7) remains very similar from the outer rings towards the centre of the closure ($R' = 0.84$). (bi) Map of bulls-eye-fold pattern through steep to sub-vertical sheath folds developed in Lewisian orthogneiss, Badcall Bay, (NC14924110). The individual layers show limited variation in thickness (T_{yz} 2.08) whilst the elliptical ratio (R_{yz} 1.94) decreases from the outer rings towards the centre of the closure (R' 1.06). (bii) Map of bulls-eye-fold in sub-horizontal sheath folds developed in Moine psammite, Creag Ruadh, (NC6969463114). The individual layers show limited variation in thickness (T_{yz} 2.4) whilst the elliptical ratio (R_{yz} 2.6) decreases from the outer rings towards the centre of the closure (R' 1.15). (ci) Map of cats-eye-fold within Moine psammites at Skullomie (NC6214661843). The individual layers show a marked variation in thickness (T_{yz} 5.2) whilst the elliptical ratio (R_{yz} 6.1) displays a progressive increase from the outer rings towards the centre of the closure (R' 0.76). (cii) Map of cats-eye-fold within Moine psammites SE of Loch Cormac (NC6329257624). The individual layers show a marked variation in thickness (T_{yz} 4.42) whilst the elliptical ratio (R_{yz} 4.13) displays a progressive increase from the outer rings towards the centre of the closure (R' 0.52).

5.12) and marked variations in layer thickness (T_{yz} 4.81) (Fig. 2ci, cii). The studied folds also display hinge apical angles (β) of $\sim 90^\circ$ associated with tight inter-limb angles (α) of $<20^\circ$. Thus, these cats-eye-folds are marked by tighter inter-limb angles than the case study Type A folds, despite the cats-eye-folds displaying apical angles (β) more than double that of the analogous-eye-folds!

The observation noted above questions the widely held assumption that progressive inter-limb tightening and associated axial planar rotation (towards the shear plane) will occur in tandem with sequential hinge rotation (towards the shear direction). Clearly this view is largely based on the traditional concept of sheath folds developed during progressive simple shear deformation (Cobbold and Quinquis, 1980). According to such models, sheath folds with smaller apical angles (β) should also display tighter inter-limb angles (α). Our observations, together with the variable relationships between inter-limb angles and hinge orientations recorded elsewhere (e.g. Fossen and Rykkelid, 1990; Fossen and Holst, 1995) suggest that models of fold hinge rotation and sheath folding should not be restricted to simple shear deformation but should also incorporate more general shear and constrictional types of deformation. Jiang and Williams (1999) have reviewed the theoretical development of sheath folds in different shear zone settings. They conclude that sheaths are most likely to develop in association with simple shear, or alternatively in shear zones

marked by constrictional non-coaxial deformation. We shall now examine examples of natural sheath folds developed during simple shear, general shear and constrictional shear and directly compare the geometry of resulting eye-folds in terms of elliptical ratios (R_{yz}), eye-fold patterns (R') and thickness variations (T_{yz}) in each of these major settings. Determination of bulk strain type is based on our own observations, together with the original authors description of strain types and fabric patterns.

3. Sheath folds generated during simple shear deformation

Over the past three decades progressive simple shear deformation has been invoked by numerous authors as the ''classic'' model to account for the generation of sheath folds. Within such a scenario gently curving fold hinges that may either entirely pre-date, or form early in the shearing event are progressively rotated towards the shear direction (Cobbold and Quinquis, 1980; Ramsay, 1980). Such rotations are a geometric artifact of intense deformation ($\gamma > 10$) and may result in an entirely passive amplification of mildly curvilinear hinge-lines into sheath folds. In simple shear, the fold amplitude (measured along Z) and the length of the hinge-line span (measured along Y) remain constant by definition (Cobbold and Quinquis, 1980).

3.1. Criteria for distinguishing simple shear deformation associated with sheath folds

Sheath fold data have been drawn from a host of authors who describe a combination of features that leads them to independently suggest that deformation and bulk strain is indeed dominated by simple shear. These criteria typically include the presence of intense planar foliations and lineations associated with S–L tectonic fabrics (e.g. Gaudemer and Tapponier, 1987; Boyle and Dawes, 1991), together with general grain shape fabrics (e.g. Vollmer, 1988; D'el Rey Silva and Barros Neto, 2002) and the geometry of pressure shadows around rigid inclusions (e.g. Quinquis et al., 1978; Salinas-Prieto et al., 2000). The presence of C–S fabrics is also regarded as probably reflecting simple shear deformation (e.g. Passchier and Trouw, 2005, p. 131) and has been recognised by a number of authors in association with simple shear-generated sheath folds (e.g. McCourt and Vearncombe, 1987; Searle et al., 2004). Several authors, in conjunction with other criteria, also provide strain studies related to sheath folds indicating plane strain associated with simple shear. These analyses have been conducted on a variety of markers including accretionary lapilli (e.g. Mukhopadhyay and Matin, 1993), quartz grains and pebbles (e.g. Malavieille, 1987a,b), and deformed porphyroblasts (e.g. Goscombe, 1991). Classic sigmoidal shear zone patterns (e.g. Evans and Neves, 1992), coupled with large-scale rotation of originally orthogonal bodies (e.g. dykes and ore feeder zones into sub-parallelism with sheared margins, Boyle, 1987), have also been used to invoke simple shear-dominated deformation. The analysis of deformed lineation patterns around later sheath folds, coupled with asymmetric porphyroclasts tails, is also consistent with, and supports simple shear in some instances (e.g. Srivastava, 2001). Although individually, such criteria and observations may simply be taken to support non-coaxial deformation, when taken in combination with the range of features recorded by authors, they collectively indicate the dominance of simple shear deformation.

3.2. Analysis of sheath folds generated during simple shear

Our analysis of sheath folds generated during simple shear reveals that the vast majority (>99%) display cats-eye-fold patterns (mean R' 0.692, Table 1). Typical examples of such cats-eye-folds generated during simple shear deformation are illustrated in Fig. 3a–h. Asymmetric *tear-drop* patterns of some folds (e.g. Fig. 3a, f, g) are considered to reflect the variable orientations of hinge-lines on either side of the eye relating to fold hinge-line vergence (see Alsop and Holdsworth, 1999, 2004a,b). Sheath folds associated with simple shear typically display pronounced elliptical ratios (R_{yz} 5.46, Table 1) and plot on a distinct trend on graphs displaying y–z sheath axes (Fig. 6a). Inner and outer ellipses plot on slightly different trends, with the inner ellipse displaying more pronounced/extreme elliptical ratios ($R_{y'z'}$ 6.96, Table 1) reflecting the overall cats-eye-folding (Fig. 6a, b). Plots comparing the inner ($R_{y'z'}$) and outer (R_{yz}) elliptical ratios of sheath folds generated during simple shear also display a distinct pattern on %frequency plots with 98% of inner ($R_{y'z'}$) and 93% of outer (R_{yz}) elliptical ratios typically greater than 3 also reflecting cats-eye-folding ($R' < 1$) (Fig. 6b, Table 1).

Table 1
Parameters recorded from sheath folds developed during different deformation conditions

	Overall sheath folds ($N = 1425$ from 501 sheaths)	Simple shear sheath folds ($N = 380$ from 160 sheaths)	General shear sheath folds ($N = 362$ from 137 sheaths)	Constrictional sheath folds ($N = 344$ from 124 sheaths)	Tubular sheath folds ($N = 203$ from 49 sheaths)
Elliptical ratio	4.600	5.464	7.012	2.220	4.065
Mean R_{y-z}	4.181	4.614	5.759	2.421	3.677
Mean $R_{y'-z'}$	5.808	6.955	8.795	1.998	4.470
Mean R'	0.854	0.692	0.691	1.234	0.850
Mean T_{yz}	3.539	3.307	4.347	2.937	3.608

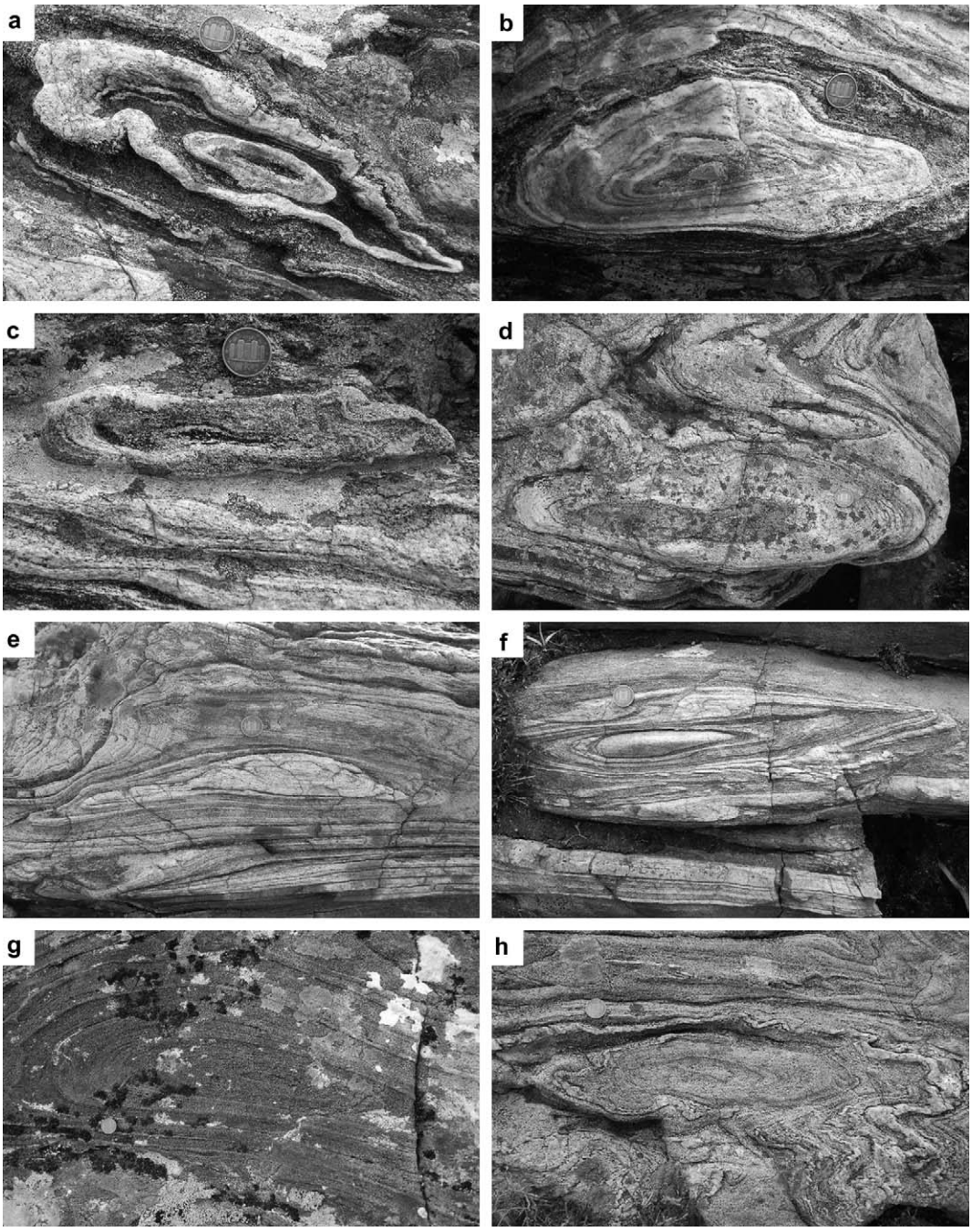

Fig. 3. Photographs of sheath folds developed during simple shear deformation (coin is 15 mm diameter in each case). Images are viewed directly down-plunge of the sheath x axes to enable calculation of elliptical ratios (R_{yz}) and R'. Sheaths showing cats-eye-folds from Moine psammite SE of Loch Cormac displaying (a) (R_{yz} 4.13) (R' 0.52) (NC6329257624) (see Fig. 2cii), (b) (R_{yz} 2.73) (R' 0.62) (NC6329257624), (c) (R_{yz} 5.13) (R' 0.61) (NC6329257624), (d) (R_{yz} 3.33) (R' 0.53) (NC6296257836). Photographs of more pronounced cats-eye-folds developed within Moine psammite at Skullomie displaying (e) (R_{yz} 6.4) (R' 0.828) (NC6200661578), (f) (R_{yz} 6.1) (R' 0.76) (NC6214661843) (see Fig. 2ci), together with less-pronounced elliptical ratios at Dalcharn, (g) (R_{yz} 3.77) (R' 0.45) (NC6235358570), (h) (R_{yz} 3.5) (R' 0.47) (NC6235358570).

4. Sheath folds generated during general shear deformation

General non-coaxial flow, associated with a regional component of pure shear, has been suggested in the development of sheath folds by several authors (Holdsworth and Roberts, 1984; Patrick, 1988; Menardi-Noguera, 1988; Tabor and Hudleston, 1991; Stauffer and Lewry, 1993; Seno et al., 1998; Ghosh et al., 1999; Carosi and Oggiano, 2002) with most authors recognising little or no finite extension along the intermediate (Y) axis, i.e. approximately plane strain ($k = 1$). Yassaghi et al. (2000) note that sheath folds may be partially dismembered by shear zones which cut through fold limbs and are marked by an overall general shear incorporating both non-coaxial and flattening ($k < 1$) strains.

4.1. Criteria for distinguishing general shear deformation associated with sheath folds

Authors from whom our sheath fold data have been drawn independently suggest general shear marked by a component of pure shear flattening based on a number of distinguishing structures and combination of features. These criteria typically include the presence of intense planar foliations associated with S and S > L tectonic fabrics (e.g. Klepeis et al., 1998; Boettcher and Mosher, 1998), together with the development of $k < 1$ strain marked by oblate enclaves, mineral aggregates and pebble fabrics (e.g. Teyssier et al., 1988; Daigneault et al., 1990; Tabor and Hudleston, 1991). Opposing senses of shear on either margin of less deformed augen, coupled with conjugate minor shear zones have also been taken as reflecting general shear (e.g. Koestler, 1988). Compaction of porphyroblast wings around adjacent porphyroblasts (e.g. Stauffer and Lewry, 1993), combined with general flattening of fabrics around porphyroblasts (e.g. Sengupta and Ghosh, 2004), have been interpreted as reflecting general shear marked by additional pure shear components. Whilst some authors find no evidence for extension along the *Y* axis of the finite strain ellipsoid (e.g. Holdsworth and Roberts, 1984; Diez Balda et al., 1995), others note variable extension along the *Y* axis coupled with greater extension along *X* (e.g. Kusky and Bradley, 1999; Mvondo et al., 2003). These relationships may be supported by the growth along *Y* of aligned mineral fibres (e.g. Faure, 1985; Menardi-Noguera, 1988). Analysis of quartz *c*-axis patterns in areas that have undergone simple shear combined with a pure shear component reveals Type 1 crossed girdle *c*-axis patterns. These (in combination with other criteria) may be interpreted as reflecting a coaxial component to the deformation (Schmid and Casey, 1986) (e.g. Tabor and Hudleston, 1991; Diez Balda et al., 1995; Mvondo et al., 2003). The analysis of deformed lineation patterns around later sheath folds, coupled with general flattening around porphyroblasts, is also consistent and supports general shear in some instances (e.g. Ghosh et al., 1999; Sengupta and Ghosh, 2004). Clearly, an increasing pure shear component within the general shear will result in progressively more of these features being developed. Once again, most authors who have observed sheath folds combine a variety of these criteria when suggesting a general shear incorporating both simple and pure shear components.

4.2. Analysis of sheath folds generated during general shear

Our analysis of sheath folds generated during general shear reveals that the vast majority (>99%) display cats-eye-fold patterns (mean R' 0.691, Fig. 6c, d, Table 1). Typical examples of such cats-eye-folds formed during general shear deformation are illustrated in Fig. 4a–h. Double-vergence geometries are developed around some eye-folds (e.g. Fig. 4g) reflecting opposing sense of hinge rotation on either margin of the eye (see Alsop and Holdsworth, 2004b). Sheath folds generated during simple and general shear are, as may be anticipated, geometrically similar to one another, but with a number of important differences. Sheath folds generated during general shear display greater mean elliptical ratios (7.01 compared to 5.46 with simple shear), higher R_{yz} (5.76) and $R_{y'z'}$ (8.8) compared to R_{yz} (4.61) and $R_{y'z'}$ (6.96) simple shear sheath folds (Table 1). The difference in axial ratios of sheath folds in simple shear and general shear settings are most clearly displayed on plots of *y* and *z* axes of individual sheath folds (Fig. 6a, c). Sheath folds generated during general shear plot on a lower trajectory to simple shear-dominated sheaths (Fig. 6a, c). This lower trend reflects the increased component of pure shear across the shear zone. However, the R' value (R' 0.69) is identical to sheath folds generated during simple shear sheaths possibly suggesting that R' reflects original geometrical relationships of pre-cursor periclinal folds (Fig. 6b, d, Table 1, see below). Sheath folds forming under conditions of intense simple shear, with or without components of pure shear, clearly display marked variations in the resultant axial ratios and elliptical patterns. Plots comparing the inner ($R_{y'z'}$) and outer (R_{yz}) elliptical ratios of sheath folds generated during general shear also display a distinct pattern on %frequency plots with 98% of inner ($R_{y'z'}$) and 97% of outer (R_{yz}) elliptical ratios typically greater than 3 (Fig. 6d, Table 1).

5. Sheath folds generated during constrictional shear deformation

The development of sheath folds in overall constrictional regimes marked by shortening in both the *Y* and *Z* directions of the finite strain ellipsoid has been suggested and reported by a number of authors (e.g. Mattauer et al., 1981; Fletcher and Bartley, 1994; Vassllo and Wilson, 2002; Terry and Robinson, 2003). However, the precise role of constriction remains uncertain as typically irregular domes and basins developed in the early stages of constrictional experiments do *not* evolve into sheath folds with further progressive shortening (Ghosh et al., 1995, p. 1367). Constrictional deformation may of course act upon pre-existing folds resulting in the development of sheath folds.

Although Hansen (1971) believed outcrop-scale conical folds in the Trollheimen area of Norway to be dome and basin structures created by the interference of two separate fold phases, there is no evidence of fabric superposition and we therefore reinterpret this superbly detailed work as reflecting continuous folding during progressive deformation. Indeed, Hansen (1971, p. 112) does suggest that curvilinear folds that display similar profiles developed during constrictional deformation associated with convergent flow patterns.

5.1. Criteria for distinguishing constrictional deformation associated with sheath folds

Authors from whom our data have been drawn independently suggest constrictional deformation associated with the development of sheath folds based on a number of distinguishing structures and combination of features. These criteria typically include the presence of L and L > S tectonites and

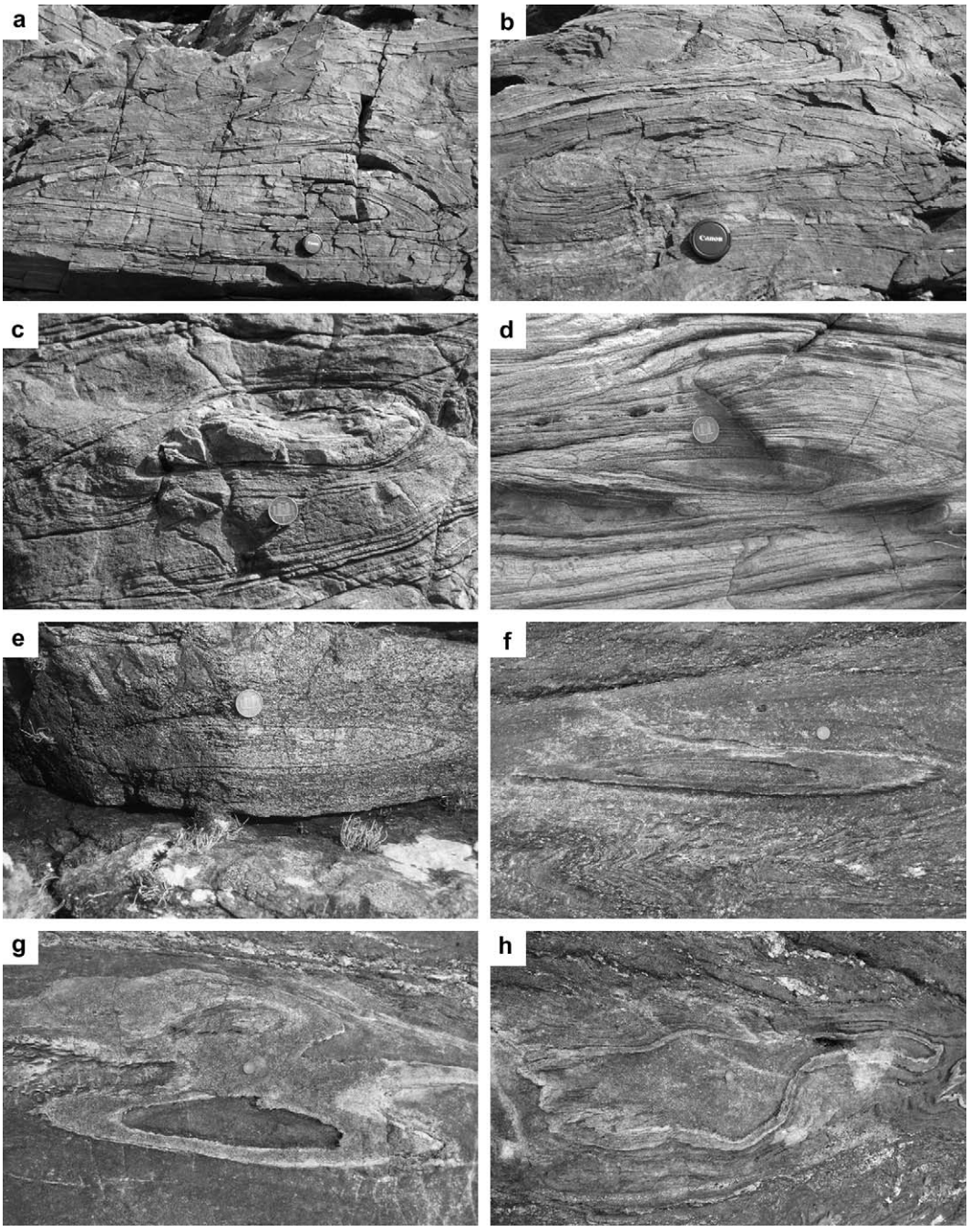

Fig. 4. Photographs of sheath folds developed during general shear deformation (lens cap is 60 mm diameter in (a) and (b), coin is 15 mm diameter in (c)–(h)). Images are viewed directly down-plunge of the sheath x axes to enable calculation of elliptical ratios (R_{yz}) and R'. Sheaths showing cats-eye-folds from Moine psammite at Sleiteil displaying (a) (R_{yz} 5.7) (R' 0.57) (NC6270162957), (b) (R_{yz} 4.9) (R' 0.64) (NC6270162957), (c) (R_{yz} 3.0) (R' 1) (NC6268962929) (see Fig. 2ai), (d) (R_{yz} 6.8) (R' 0.932) (NC6269762844). (e) Clashnessie Bay Lewisian orthogneiss (R_{yz} 8.3) (R' 0.66) (NC05753140). Pronounced cats-eye-folds developed within Moine psammite at Loch Quoich displaying, (f) (R_{yz} 9.2) (R' 0.68) (NH0147604056), (g) (R_{yz} 5) (R' 0.58) (NH0147604056), (h) (R_{yz} 4.7) (R' 0.84) (NH0147604056) (see Fig. 2aii).

generation of quartz rods (e.g. Chadwick, 1990; Oliver, 1994; Vassllo and Wilson, 2002), together with the development of $k > 1$ strain marked by prolate enclaves, mineral aggregates and pebble fabrics (e.g. Mattauer et al., 1981; Diez Balda et al., 1995; Poli and Oliver, 2001; Merschat et al., 2005). The pronounced linear character of the rocks may also be enhanced by the marked alignment of cylindrical fold hinges and mineral lineations (e.g. Mukhopadhyay and Sengupta, 1979; Schulmann et al., 1994; Kelly et al., 2000; Beunk and Page, 2001). Shortening along the Y axis of the finite strain ellipsoid, coupled with greater shortening along Z, has also been recorded (e.g. Azcarraga et al., 2002) and has been supported by the growth of aligned crystal fibres within pressure shadows (e.g. Cluzel et al., 1991). Constrictional deformation

associated with sheath folding may result in converging fabrics related to variably orientated axial planes (e.g. Veenhof and Stel, 1991; Terry and Robinson, 2003). It has also been noted that layer thickness around sheath folds may display only limited variation and such folds may therefore be generated by constriction (e.g. Ez, 2000). Most authors employ a variety of these criteria when distinguishing bulk constrictional deformation associated with sheath folds.

5.2. Analysis of sheath folds generated during constrictional shear

Our analysis of sheath folds generated during constrictional shear reveals that the vast majority (>92%) display bulls-eye-fold patterns (mean R' 1.23, Fig. 6e, f, Table 1). Typical examples of such bulls-eye-folds formed during constrictional shear are illustrated in Fig. 5a–h and are marked by pronounced

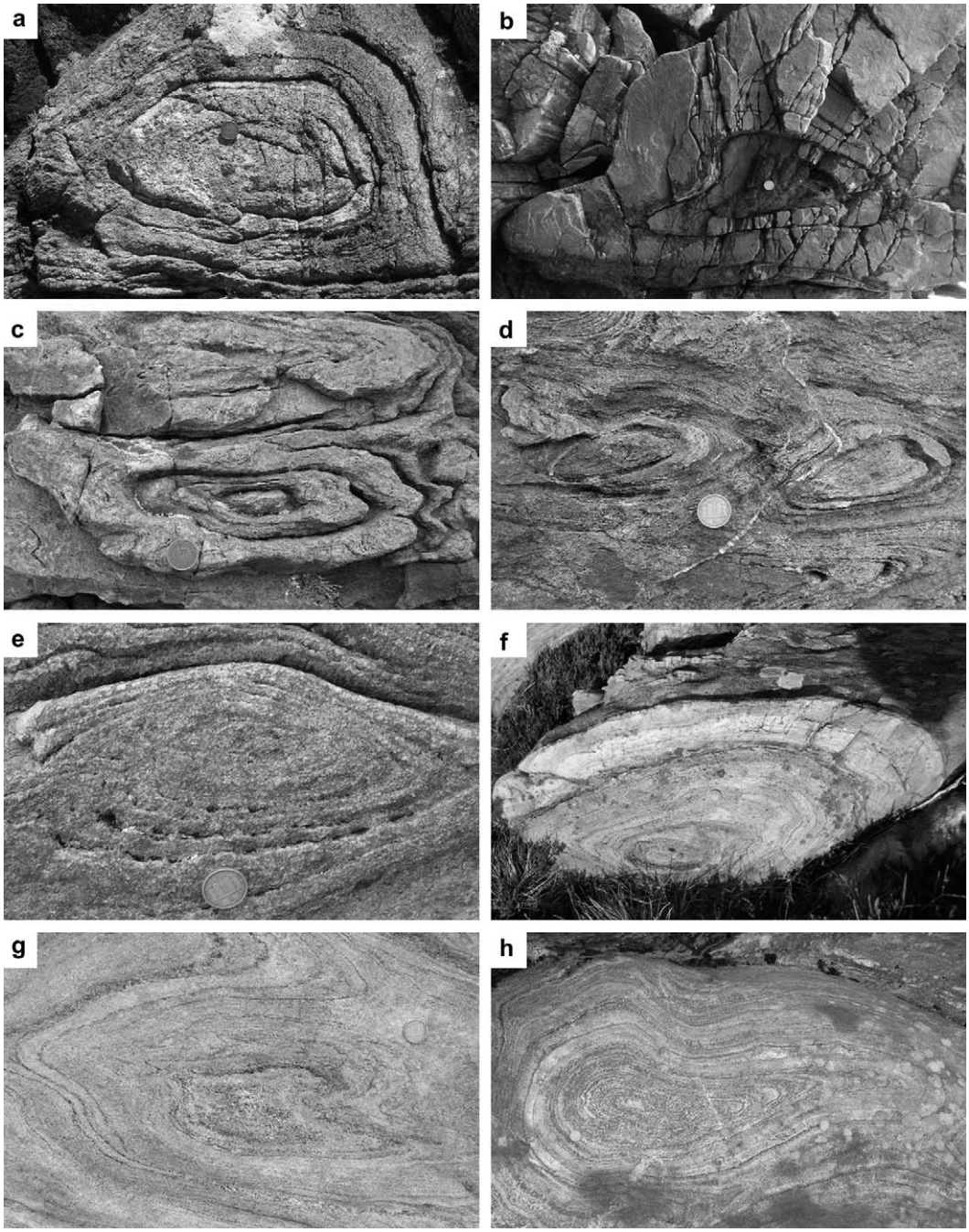

Fig. 5. Photographs of sheath folds developed during constrictional deformation (coin is 15 mm diameter in each case). Images are viewed directly down-plunge of the sheath x axes to enable calculation of elliptical ratios (R_{yz}) and R'. Sheaths displaying bulls-eye-folds from (a) Lewisian orthogneiss at Badcall Bay (R_{yz} 1.94) (R' 1.06) (NC14924110) (see Fig. 2bi). Sheaths from Moine psammites with amphibolite at (b) Creag Ruadh (R_{yz} 2.6) (R' 1.15) (NC6969463114) (see Fig. 2bii). Sheaths from Moine psammite at Melness displaying (c) (R_{yz} 4.04) (R' 1.21) (NC58476455), (d) (R_{yz} 2.4) (R' 1.03) (NC58476455), (e) (R_{yz} 2.6) (R' 0.86) (NC58516454), (f) Sleiteil (R_{yz} 2.2) (R' 1.02) (NC6295362512). Bulls-eye-folds are preserved within Moine psammites at Loch Quoich, (g) (R_{yz} 2.6) (R' 1.22) (NH0437901738), (h) (R_{yz} 2.5) (R' 1.36) (NH0437901738).

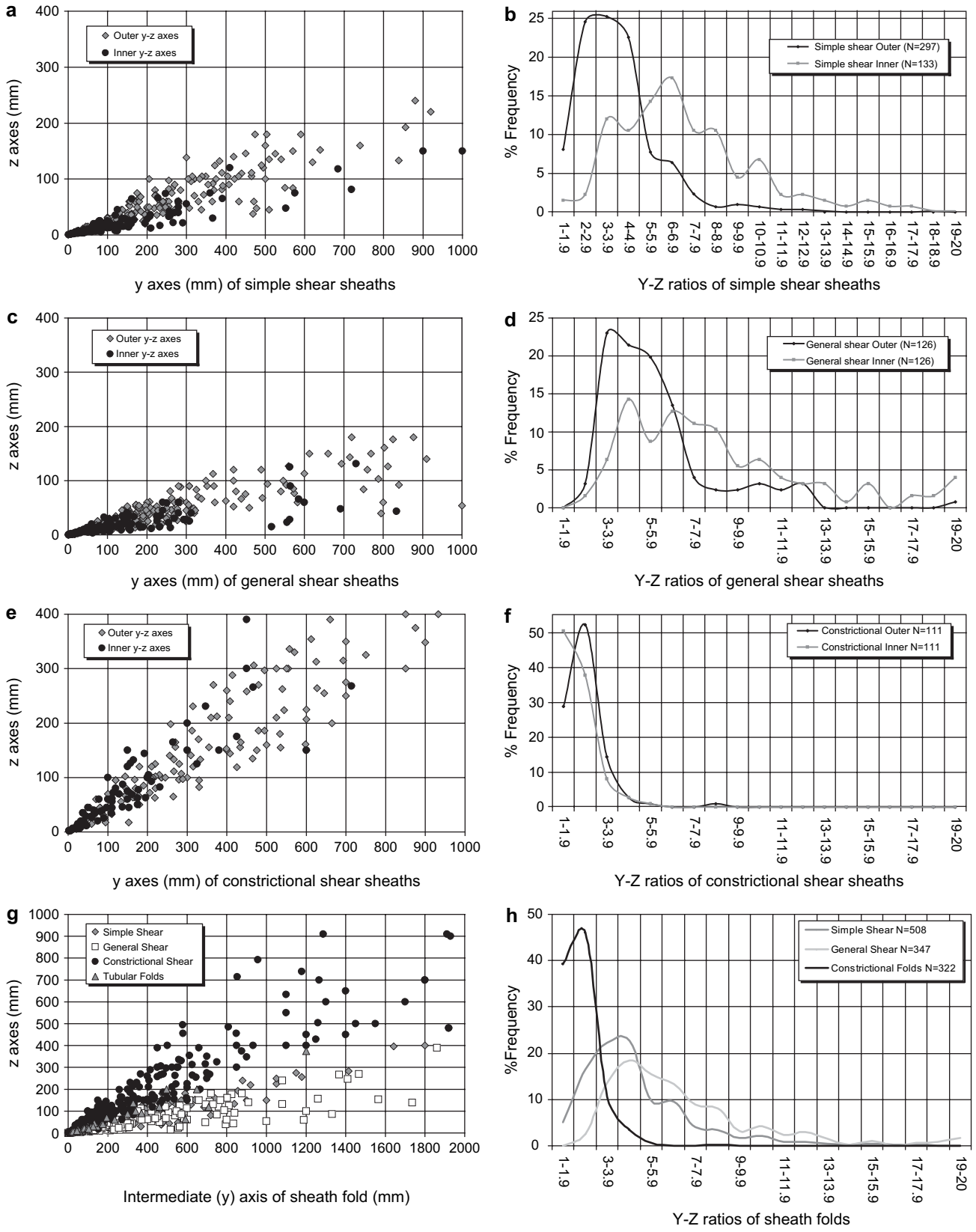

Fig. 6. Measurements (mm) of y and z axes of individual sheath folds (left) and %frequency curves of outer-most and inner-most elliptical ratios (right) for sheaths developed during simple shear (a,b), general shear (c,d) and constrictional shear (e,f). Data from each individual sheath is divided into outer-most y–z axes (R_{yz}) (grey diamonds) and inner-most y–z axes ($R_{y'z'}$) (black circles). Plots and %frequency curves of all y–z data from simple shear, general shear and constrictional shear sheath folds, as well as tubular folds, are shown in (g) and (h). Note how sheaths generated during constriction display a different trend to those generated during simple/general shear. Our own observations with additional data from a range of authors are available from the online version of this article (see Appendix).

mineral elongation lineations that plunge directly through the fold closure and bisect the bulls-eye-fold. Sheath folds associated with constrictional deformation display low elliptical ratios (mean 2.22, Fig. 6f, Table 1) and plot as a distinct trend on graphs displaying $y-z$ sheath axes (Fig. 6e). Plots comparing the inner ($R_{y'z'}$) and outer (R_{yz}) elliptical ratios of sheath folds generated during constrictional shear also display a distinct pattern on %frequency plots with 90% of inner ($R_{y'z'}$) and 83% of outer (R_{yz}) elliptical ratios typically less than 3 (Fig. 6f, Table 1). Very few (2.7%) constrictional sheath folds exceed elliptical ratios (R_{yz}) of 4 with <1% of inner bulls-eye pupils ($R_{y'z'}$) exceeding this value compared to >90% in sheaths formed during simple/general shear.

6. Tubular folds

A distinct class of extreme sheath fold where the hinge-line bends through more than 160° and displays xy ratios >1 has been termed tubular folds (Skjernaa, 1989). Williams and Zwart (1977, p. 180) had previously recognised that ''tubular folds can only be explained by relative movement of component elements parallel to the tube axis and thus parallel to the lineation''. Skjernaa considered tubular folds to develop from periclinal folds that initiate sub-parallel to the shear direction, rather than sub-normal as is typically assumed for classic sheath folds. Our analysis and comparison of the tubular fold data set of Skjernaa (1989) with sheath folds generated during simple shear reveals a number of similarities. The vast majority (>99%) of tubular folds display cats-eye-fold patterns marked by slightly lower elliptical ratios (mean R_{yz} 4.07) but greater R' values (R' 0.850) than simple shear sheath folds (Table 1). Tubular folds do not appear to define a distinct ''field'' or ''trend'' on plots and most clearly overlap with sheath folds generated during simple shear (Fig. 6g).

7. Geometric comparison of sheath folds generated in different strain settings

The y and z axes of individual sheath folds generated during simple shear, general shear and constrictional deformation are directly compared in Fig. 6g. These graphs show that sheath folds generated during constriction plot on a quite different trend to those formed during simple and general shear, reflecting the lower elliptical ratios of sheaths created during constriction. This relationship is also clearly illustrated on %frequency plots of overall $y-z$ ratios of sheath folds with 94% of simple shear-generated sheaths and 98% of general shear sheaths displaying $R_{yz} > 3$, whilst conversely, 86% of sheaths formed in constrictional shear display $R_{yz} < 3$ (Fig. 6h).

Variations in outer (R_{yz}) and inner ($R_{y'z'}$) elliptical ratios resulting in Type A ($R' = 1$) analogous-eye-folds, Type B ($R' > 1$) bulls-eye-folds, and Type C ($R' < 1$) cats-eye-folds may be compared on an *eye-chart* (Fig. 7). The inner ($R_{y'z'}$) and outer (R_{yz}) elliptical ratios of individual sheath folds generated during simple shear, general shear or constrictional deformation may thus be directly plotted and display distinct

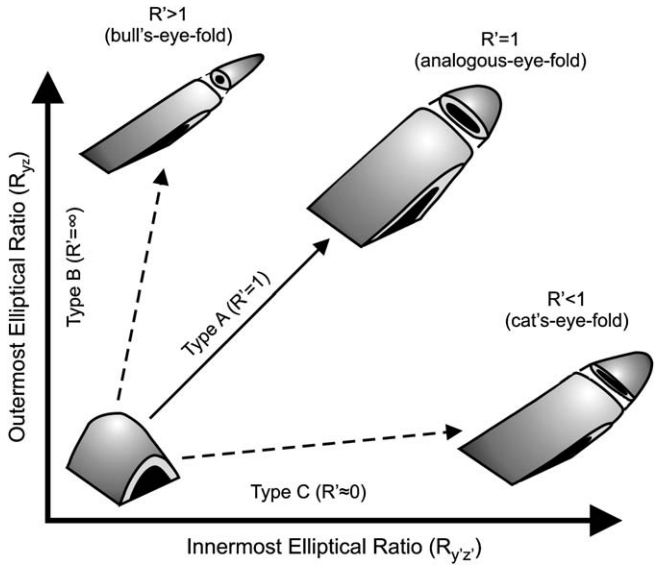

Fig. 7. Summary eye-chart illustrating variations in outer (R_{yz}) and inner ($R_{y'z'}$) elliptical ratios resulting in Type A ($R' = 1$), analogous-eye-folds, Type B ($R' > 1$), bulls-eye-folds, and Type C ($R' < 1$), cats-eye-folds. Schematic sheath folds generated from the initial fold structure at the origin are shown for each scenario. See text for further discussion.

trends on such *eye-charts* (Fig. 8a). Simple shear and general shear sheaths (together with tubular folds) clearly overlap with one another resulting in almost identical mean trend lines across a wide range of elliptical ratios (Fig. 8a). Sheath folds formed during constriction, however, display a markedly different trend associated with lower elliptical ratios and reflecting bulls-eye-folds (Fig. 8a).

The variation in overall aspect ratios from outer to inner rings is defined as R' (where $R' = R_{yz}/R_{y'z'}$) and this value may be directly compared with the elliptical ratios of the inner-most ellipses of individual sheaths (Fig. 8b). This plot illustrates that during both simple shear and general shear, there is no significant variation in R' when the inner-most ($R_{y'z'}$) aspect ratios >6. However, where aspect ratios are <6, then a progressive increase in R' is recorded as the $R_{y'z'}$ values decrease (Figs 8b). This reflects an overall increasing self-similarity between inner and outer ellipses with lower elliptical ratios. The R' values of sheath folds generated during simple shear and general shear show very similar %frequency profiles, with identical mean values of R' 0.69. This suggests that R' cats-eye-folds are not controlled by the amount of deformation or an increasing pure shear component in general shear.

Sheath folds generated during constrictional deformation typically display $R' > 1$ reflecting Type B or bulls-eye-folds that may be directly compared with the elliptical ratios of the inner-most ellipses of individual sheaths (Fig. 8b). The most pronounced bulls-eye-folds are displayed by sheaths with moderate outer elliptical ratios (R_{yz} 2–3) and sub-circular inner-eyes or pupils ($R_{y'z'}$ 1–2) (Fig. 8b). Thus, sheaths developed during constriction display markedly lower elliptical ratios (96% of sheaths display $R_{yz} < 3.9$) but greater R' values

than those generated during simple/general shear (95% of sheaths display $R_{yz} > 3$).

The thickness of individual marker layers within eye-folds may be measured along the y axis (parallel to the axial surface) (t_y) and at 90° to this along the z axis (t_z) to define the ratio of T_{yz} (Fig. 1). Measurements of t_y and t_z for individual layers may then be directly compared (Fig. 8c). Layering within sheath folds generated during simple shear and general shear display higher ratios between t_y and t_z and plot on a flatter trajectory than sheaths generated during constriction. Constrictional eye-folds display less variation between t_y and t_z for any individual layer thus reflecting more equant layer thickness around the fold. Sheath folds generated within simple shear and general shear typically display $T_{yz} < 4$ with means of T_{yz} 3.31 and T_{yz} 4.35, respectively (Table 1). Elliptical ratios do not display a strong direct correlation with T_{yz}, although $R_{yz} < 4$ tend to be associated with less variation in layer thickness ($T_{yz} < 3$). Sheath folds generated during constriction display lower T_{yz} values with a mean of T_{yz} 2.94 (Table 1). Constrictional sheaths displaying $T_{yz} > 4$ also show a slight tendency towards greater elliptical ratios ($R_{yz} > 3$).

Marker layers may also be described as a proportion of the overall sheath y axis (y'/y) and z axis (z'/z) (Fig. 8d). This has the advantage that the normalised ratio is independent of scale and therefore more clearly reflects the sequential variation in layer shape with progressive changes in elliptical ratios towards the centre of the sheath. For sheath folds created during simple shear and general shear, y'/y values are greater than z'/z whilst the converse is true for constrictional sheaths (Fig. 8d). This relationship simply records the predominance of cats-eye and bulls-eye-fold geometries in each of these settings, respectively. Subtracting the y'/y ratio from the z'/z ratio for each sheath fold provides a single value ($R'_z - R'_y$) which reflects the *relative* change in length of y and z axes. Sheaths created during simple shear and general shear display normal distribution patterns which broadly coincide with one another peaking at values of −0.1 whilst sheaths generated during constriction display +ve values (Fig. 8e). Constrictional sheaths with the highest ($R'_z - R'_y$) ratios typically correspond to those with the greatest R' values (Fig. 8f) reflecting more pronounced bulls-eye-folds. The converse is true of sheath folds generated during simple/general shear where the most negative ($R'_z - R'_y$) ratios are associated with the lowest R' values and most pronounced cats-eye-fold patterns (Fig. 8f). These various plots of individual folds clearly distinguish layer thickness changes associated with cats-eye and bull-eye-folds and may be used to differentiate folds formed during constriction and simple/general shear.

8. Quantitative strain data and sheath folds

Strain analysis associated with computer simulation of sheath folds has been undertaken by Vollmer (1988) who assumed simple shear deformation, and Seno et al. (1998) who invoke a general shear. Such a combination of simultaneous pure and simple shear resulted in the generation of curvilinear sheath folds at much lower values of shear strain ($\gamma = 2$) than modelled for simple shear alone ($\gamma > 5$: Cobbold and Quinquis, 1980). Prolate finite strains associated with apparent constriction are recorded in the noses of km-scale sheath folds whilst the limbs are marked by oblate strain and apparent flattening (Seno et al., 1998, figs. 1 and 3). Although this pattern was interpreted by Seno et al. (1998) as a later phase of deformation, the broad variation is in agreement with *c*-axis fabric measurement recorded around minor sheath folds by Crispini and Capponi (1997) in which oblate strains on the limbs give way to plane and prolate strains on the nose and hinges of the sheath, respectively.

Quantitative strain data in rocks affected by sheath folding has been collected in a number of deformation regimes broadly interpreted as being dominated by simple shear (e.g. Malavieille, 1987b; Goscombe, 1991; Mukhopadhyay and Matin, 1993), general shear (e.g. Lacassin, 1983; Faure, 1985; Menardi-Noguera, 1988; Teyssier et al., 1988; Daigneault et al., 1990; Tabor and Hudleston, 1991; Stauffer and Lewry, 1993; Diez Balda et al., 1995; Yassaghi et al., 2000), or constrictional deformation (e.g. Mattauer et al., 1981; Veenhof and Stel, 1991; Poli and Oliver, 2001; Beunk and Page, 2001; Vassllo and Wilson, 2002; Terry and Robinson, 2003; Merschat et al., 2005). Within simple shear-dominated examples, the calculated mean k value is close to 1 ($k = 1.22$) whilst associated sheath folds display mean elliptical ratios (R_{yz}) of 4.5, 7.3, T_{yz} 2.68 and $R' = 0.67$ (Fig. 8g, h). Within general shear, the addition of a pure shear flattening component results in a lower mean k value ($k = 0.67$), greater aspect ratios of R_{yz} 6.9, $R_{y'z'}$ 11.2 and T_{yz} 4.68, but the associated sheath folds still display $R' = 0.65$ similar to that of sheaths within simple shear (Fig. 8g, h). Sheath folds developed in regimes where flattening is more pronounced and $k < 0.75$ display greater T_{yz} values (T_{yz} 5.213) compared to where $k > 0.75$ (T_{yz} 4.03). These relationships are further supported by the overall data sets of simple shear ($N = 380$) and general shear ($N = 362$) which provide identical mean R' values to one another. Thus, whilst the additional component of pure shear results in greater T_{yz} and R_{yz} aspect ratios, it does not appear to significantly alter the R' value.

This correlation is also demonstrated by sheath folds generated within constrictional deformation where sheaths associated with k values in the range of $k = 3$ to $k = 6$ (mean $k = 3.86$, mean $T_{yz} = 2.625$) display $R' = 1.223$, whilst sheaths associated with k values in the range of $k = 9$ to $k = 12$ (mean $k = 10.09$, mean $T_{yz} = 2.39$) display an identical mean $R' = 1.223$ (Fig. 8h). Thus, the increasing component of constrictional strain does not therefore appear to significantly alter the R' value, although the R_{yz} aspect ratio and T_{yz} value show an overall decrease with increasing k values from general shear to simple shear to constriction.

In a detailed case study, Mattauer et al. (1981) suggest that while simple shear may predominate, the finite strain ellipsoid lies within the constrictional field close to plane strain ($k = 3.6$). Our analysis of associated outcrop-scale sheath folds reveals low elliptical ratios (mean R_{yz} 1.8) and overall bulls-eye-fold patterns (mean $R' = 1.37$). Fletcher and Bartley

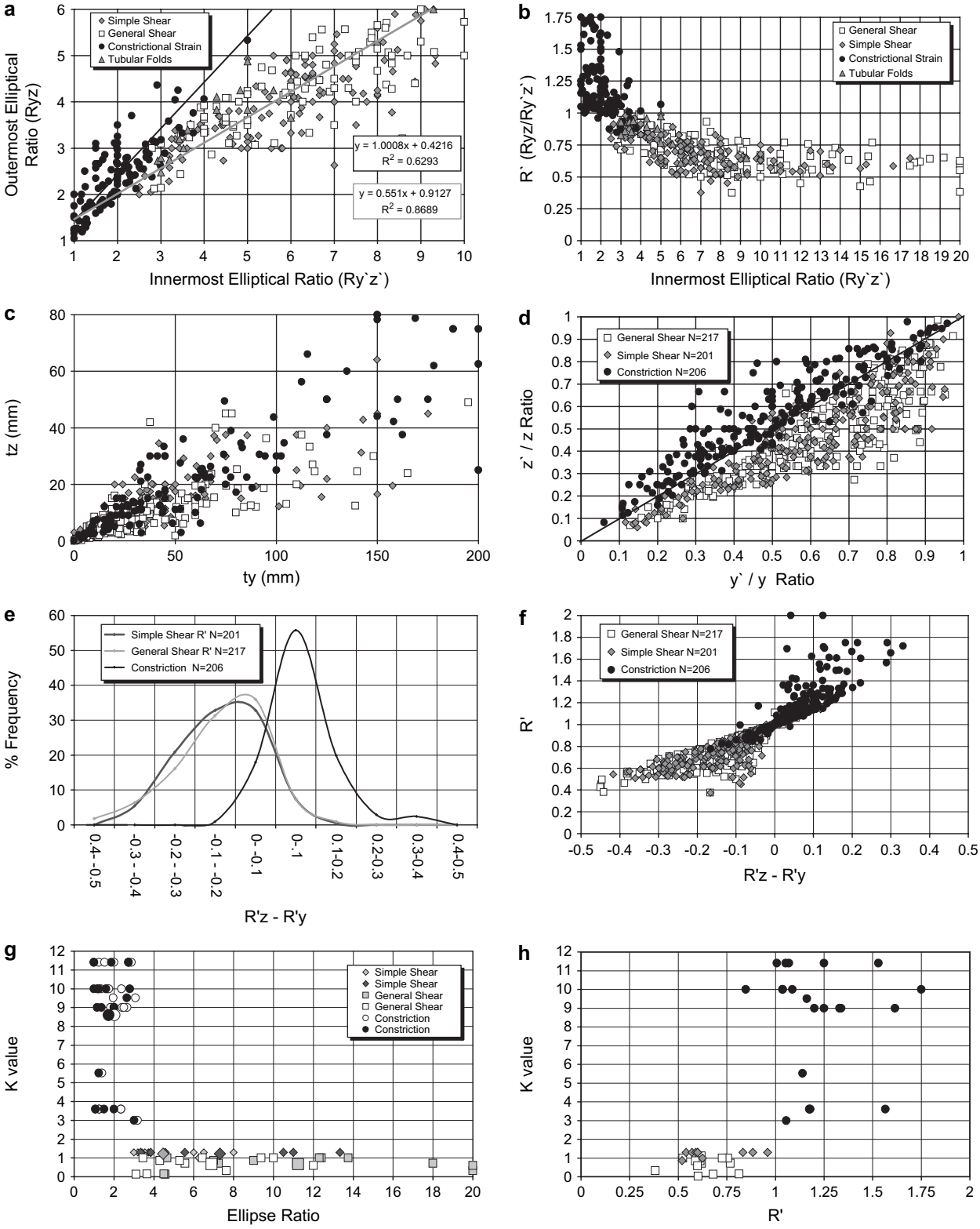

Fig. 8. (a) Eye-chart directly comparing the outer (R_{yz}) and inner ($R_{y'z'}$) elliptical ratios of individual sheath folds generated under different strain types. Note the similarities in mean trend lines for sheaths generated during simple shear and general shear when compared to that of constrictional shear, reflecting the different shapes of sheaths in each setting. (b) Chart comparing the inner ($R_{y'z'}$) elliptical ratio with R' ($R_{yz}/R_{y'z'}$). Bulls-eye-folds ($R' > 1$) are typically developed where inner and outer elliptical ratios are less than 3, whilst cats-eye-folds ($R' < 1$) are largely confined to elliptical ratios >3. Note how sheaths generated during constrictional deformation typically display lower elliptical ratios and higher R' values. (c) Plot of layer thickness (t_y and t_z) (see Fig. 1) measured along the y and z axes, respectively, of sheath folds generated during simple shear (grey diamond), general shear (open square) and constrictional deformation (black circle). Sheath folds generated during constriction typically display less extreme thinning of the limbs compared to the hinge. (d) Plot showing the inner y or z axes of individual sheaths plotted as a proportion of the outer y or z axes. Note the distinct fields associated with simple/general shear and constriction. (e) %Frequency curves for sheaths

(1994) suggest that while non-coaxial shear may be associated with plane strain ($k = 1.1$) at the grain scale, a significant component of constriction is associated with the development of transport-parallel folds. Our analysis of these sheath folds reveals calculated R_{yz} 3.44, and overall R' 1.006 bulls-eye-fold patterns. Constrictional deformation associated with an overall transtensional regime has also been invoked by Terry and Robinson (2003) in the development of minor sheath folds in Norway. Detailed plane table mapping of these folds by Terry and Robinson (2003) reveals low ratios (R_{yz} 1.67) once again associated with predominantly bulls-eye (R' 1.15) folding.

9. Discussion – what controls sheath fold geometry?

The final elliptical ratio (R_{yz}), thickness variation (T_{yz}) and R' value of any sheath fold may in part reflect a number of variables. The principal controls include (a) the type (k value) and magnitude of deformation; (b) the orientation and geometry of pre-cursor folding relative to subsequent shearing. These major controls will now be discussed together with the effects of reworking by subsequent deformation.

9.1. Variable types of deformation

As noted in the previous sections, one of the principal controls on the geometry of sheath folds appears to relate to the type of deformation. Sengupta and Ghosh (2004) record sheath folds associated with transpressional shearing in which the bulk deformation is of the flattening (or plane strain) type with the rate of stretching greater along the transport direction than the Y axis. This scenario has also been suggested as being capable of encouraging sheath fold development by Jiang and Williams (1999). Typical elliptical ratios calculated in this setting are equivalent to those observed elsewhere (R_{yz} 3.5, $R_{y'z'}$ 4.6 and R' 0.781) and similar to the overall calculated means for sheath folds generated during simple shear.

Within cats-eye-folds, inner ellipses become more pronounced when the outer ratios exceed 3, possibly reflecting inner-arc pinching during buckling of the pre-cursor folds. Cross sections through folds within high-strain zones are consistent with original buckle folds being modified during subsequent shear (Platt, 1983; Ghosh and Sengupta, 1984, 1987; Ghosh, 1993; Carreras et al., 2005). Folds that initiate with parallel geometries may during subsequent rotation approach similar fold geometries (see Carreras et al., 2005) with many sheath folds displaying similar profiles in X–Z section (Quinquis et al., 1978). Puelles et al. (2005) note that sheath folds generated during simple shear display thickened hinges and thinned limbs in both y–z and x–z sections. Simple shear acting on the pre-cursor buckle fold will not only significantly increase the curvilinearity of the fold hinge on any surface (see Ramsay, 1980), but also the thickness of layers measured along the fold axial plane. Layers in the pre-cursor fold displaying the greatest curvilinearity and hinge-thickening will thus undergo the most significant modifications during passive amplification. This suggests that the inner-most layer is more deformed (as originally recorded by Quinquis et al., 1978) and possibly reflects the nucleation and enhanced development of the core of the pre-cursor fold.

Bulls-eye-folds are typically produced where the outer elliptical ratio R_{yz} is <3, with the inner ellipse becoming even less pronounced (≪2) and displaying a more circular cross section (Figs. 5, 8a, 9). Sheath folds displaying circular R_{yz} cross sections may be generated during constrictional deformation in which the pre-cursor fold is shortened in both the Y and Z directions (e.g. Ez, 2000). Such circular sections typically display the $R' > 1$ variation from outer to inner rings demonstrated by bulls-eye-folds and so may represent one of the primary mechanism for the generation of such folds. Intense constrictional deformation may eventually result in the intermediate

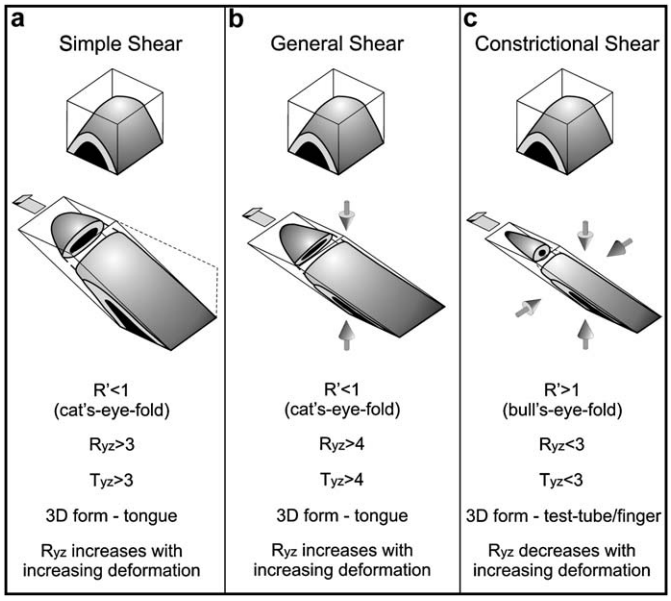

Fig. 9. Summary diagram illustrating the geometry of cats-eye and bulls-eye-folds associated with sheaths generated during (a) simple shear, (b) general shear and (c) constrictional shear. The geometry of the initial fold is shown (above) in each case, together with the geometry of deformed sheath folds resulting in tongue and test-tube forms with simple/general shear and constriction, respectively. The variation in typical measured parameters (R'), elliptical ratios (R_{yz}), and thickness ratios (T_{yz}) is also given. See text for further discussion.

generated under different strain types illustrating R'_z–R'_y (where R'_z and R'_y are the lengths of inner z and y axes calculated as proportions of the outer y and z axes, respectively). (f) $R'z$–$R'y$ (where $R'z$ and $R'y$ are the lengths of inner z and y axes calculated as proportions of the outer y and z axes, respectively) plotted against R' ratios. (g) Plots comparing k values with the elliptical ratios of inner (dark symbol) and outer (light symbol) elliptical ratios of sheath folds. Larger symbols represent calculated means for each data set comprising simple shear ($N = 10$), general shear ($N = 14$) and constrictional shear ($N = 21$). The R' values of sheath folds may be compared with the calculated k value for different strain types (h). This plot suggests that the R' value does not increase significantly with increasing k values from general shear to simple shear. Similarly, increasing k values associated with constrictional deformation do not alter the mean R' value of constrictional sheath folds. See text for discussion.

(y) and short (z) axes of the inner-most ellipse switching position relative to y and z of the outer ellipse i.e. the intermediate axis of $R_{y'z'}$ is aligned with the short axis of R_{yz}. This is a consequence of $R_{y'z'}$ possessing a lower elliptical ratio, which with increasing constriction and shortening, eventually results in y displaying a smaller value than z (e.g. Terry and Robinson, 2003). Such flipping in orientation of y and z axes in adjacent sheaths and even from the outer to inner ellipses of individual sheath folds is an indication of constrictional deformation.

It is important to note that sheaths displaying bulls-eye-folds may occasionally be found in proximity to neighbouring sheaths that show overall cats-eye geometries. This association may suggest localised strain partitioning into simple shear, general shear and constrictional-dominated domains, possibly due to the effects of differential shearing associated with flow perturbation development during general shear (e.g. Coward and Potts, 1983; Alsop and Holdsworth, 1993, 2002, 2005, in press; Alsop et al., 1996; Holdsworth et al., 2001). It may, however, also reflect additional controls on sheath fold patterns such as the geometry and orientation of original folds discussed below.

9.2. Variable orientation and geometry of pre-cursor folds

Lacassin and Mattauer (1985), Skjernaa (1989) and Mies (1993) have calculated via mathematical modelling of sheath folds within simple shear regimes that elliptical ratios (R_{yz}) are dependent on both the amount of (simple shear) deformation together with the geometry and orientation of the initial periclinal fold relative to subsequent shear. Mies (1993, p. 990) models a range of initial periclinal geometries orientated either parallel or normal to subsequent simple shear and clearly illustrates increasing R_{yz} values with increasing shear strains (γ). In addition, a relative decrease in the apical angle (β) compared to the inter-limb angle (α) of the original pericline results in greater R_{yz} values for any given value of γ, i.e. periclines displaying greater original hinge-line curvature will naturally create greater elliptical ratios (R_{yz}) for any subsequent deformation.

For the typical situation of periclines developed approximately normal to shearing, the ratio between inner and outer ellipses (R') remains constant during increasing simple shear deformation and reflects the original periclinal geometry. Conversely, original periclines orientated sub-parallel to the subsequent shear direction will display variable R' with increasing simple shear. Although bulls-eye-folds ($R' > 1$) may be developed at relatively low values of γ, the R_{yz} values rapidly increase with greater shear stain values ($\gamma > 8$). This relationship clearly distinguishes such simple shear-generated folds from those formed during constrictional deformation in which bulls-eye-folds are marked by extremely low R_{yz} values (mean R_{yz} 2.25). Thus, for any given pericline typically orientated normal to subsequent shearing, elliptical ratios (R_{yz}) will increase during increased simple shear deformation whilst R' remains constant. This study suggests that R_{yz} elliptical ratios may also be increased (whilst keeping R' constant) by increasing the pure shear component within a general shear framework.

Tubular sheath folds have been mathematically modelled by Skjernaa (1989) and Mies (1993) who both consider these intense folds to be the product of a gently-curvilinear pre-cursor fold trending parallel to the later non-coaxial shear direction (see Skjernaa, 1989; Mies, 1993 for details). Skjernaa (1989, p. 695) did, however, suggest that "a longitudinal shortening may lead to the formation of transverse folds". Ez (2000, p. 170) claims that the flow-parallel orientation of original fold orientations is a coincidence that "can not be a rule" and that such folds were probably produced by constriction. (cf. Skjernaa, 1989; Mies, 1993). Our analysis of cross sections through tubular folds reveals that they predominantly display $R' < 1$ cats-eye-fold patterns and characteristics of sheath folds generated during simple shear deformation. Conversely, mildly curvilinear pre-cursor folds trending at high angles to subsequent non-coaxial shear generate markedly curvilinear sheath folds with more pronounced R_{yz} ellipticity (Skjernaa, 1989; Mies, 1993). Cross sections through such structures consistently display $R' < 1$ cats-eye-folds.

It has long been recognised that mildly curvilinear periclinal folds display marked variations in style along the length of their fold hinge (Dubey and Cobbold, 1977). Tracing hinge-lines of individual periclines reveals increasingly angular profiles, narrower hinge zones and reduced inter-limb angles towards the culmination. These original variations in periclinal geometry may be amplified during subsequent shearing resulting in a complex range of possible sheath scenarios (e.g. see Skjernaa, 1989).

Thus, our observations, coupled with the modelling studies of Skjernaa (1989) and Mies (1993), suggest that one of the contributing factors in the development of bulls-eye and cats-eye-folds may be the orientation of the pre-cursor fold relative to the later shearing.

9.3. Variable reworking of sheath folds

Sheath folds are resilient to subsequent deformation and as such may provide a more reliable record of deformation than grain fabrics that may be readily overprinted and destroyed. Reworking of shear zone fabrics may, however, result in sheath folds themselves being refolded during continued progressive deformation or by entirely separate events (e.g. Henderson, 1981; Ghosh and Sengupta, 1984; Holdsworth, 1990; Alsop, 1992, 1994; Forbes et al., 2004). Such 3-D refold structures have been studied by a number of authors in terms of theory (e.g. Grasemann et al., 2004 and references therein) and general field analysis (e.g. Fowler and El Kalioubi, 2002). These authors suggest that the ellipticity of sheath cross sections (R_{yz}) controls the subsequent refold patterns. Shortening along the y axis of sheath folds with large R_{yz} encourages buckling of the axial plane and type-2 refolding, whilst sheaths with low R_{yz} are marked by Type 1 refolding style where the elliptical cross section becomes shortened resulting in an even lower R_{yz}. Major sheath folds ($\sim$30 km y axes) associated with prolate strains and constrictional deformation are recorded by Vassllo and Wilson (2002). Although such structures typically define small elliptical ratios (R_{yz} 2.22) associated with pronounced bulls-eye-folds (R' 1.3), sheaths

displaying variable cats-eye-fold patterns are locally preserved in areas that suffered significant later flattening strains (Vassllo and Wilson, 2002). These relationships suggest a modification of originally low R_{yz} ellipses associated with constrictional deformation by subsequent flattening strains to produce cats-eye-folds in these reworked areas. The analysis of sheath folds in areas or reworking clearly requires care, although such areas may be readily identified via overprinting fabrics and refold geometries.

9.4. Constraints of sheath folds

It has been noted that the development of sheath folds in zones of general shear is considered to be critically dependent on the direction of maximum stretching of the pure shear component compared to the direction of simple shear (Jiang and Williams, 1999). Sheath folds may be encouraged within general shear zones where these two directions coincide. However, if the stretching directions of the pure shear component and simple shear are at high angles to one another then the development of sheath folds may be impeded (Jiang and Williams, 1999). In such a scenario, folds may become more cylindrical as they rotate, with stretching parallel to hinges actually enhancing their linearity (Culshaw, 2005). Sheath folds may be considered most useful as discriminators of bulk strain where k values are close to, or greater than 1. Sheath folds are less likely to develop where the bulk strain falls well within the oblate ($k < 1$) field and as such they may be of more limited value in these settings. The notable absence of sheaths and associated eye-folds in some high-strain zones, despite evidence for hinge rotation (e.g. Mawer and Williams, 1991; Culshaw, 2005), may thus inadvertently help discriminate such ($k < 1$) strain.

9.5. Summary

Thus, the final geometry of sheath folds may in part reflect (a) the amount and type (k value) of deformation, (b) the orientation and geometry of pre-cursor folds and (c) reworking of original sheath geometries. However, our results show that 98% of sheath folds generated during simple shear and general shear display ($R' < 1$) cats-eye-fold patterns whilst >92% of sheath folds generated during constriction display ($R' > 1$) bulls-eye-folds. In addition, 98% of sheath folds formed during simple shear and general shear display inner-most elliptical ratios ($R_{y'z'}$) >3, whilst the converse is true in sheath folds generated during constriction where 90% display inner-most elliptical ratios ($R_{y'z'}$) <3 (Fig. 9). This close correlation of elliptical ratios (R_{yz}), T_{yz} values, and cats-eye or bulls-eye (R') fold patterns with simple shear, general shear or constrictional deformation very clearly suggests that the primary control on the geometry of sheath folds is the nature of the deformation regime itself (i.e. control (a)).

10. Conclusions

Sheath folds have now been carefully documented by a host of authors. Analysis of this published work, together with our own observations, allows us to make some general remarks and draw some conclusions about sheath fold geometries and deformation. This study demonstrates that:

(a) Folds in general, and sheath folds in particular, provide a more complete record of the deformation history than fabrics that are more readily transposed and ''reset''. Eye-folds, representing y–z cross sections across sheaths, are not easily destroyed and may provide a more reliable indicator of bulk strain type than some traditional techniques that may be subject to problems of matrix-clast viscosity contrasts etc.

(b) A new descriptive framework has been established which allows eye-folds to be defined according to the elliptical (y–z) ratios of the outer- (R_{yz}) to the inner-most ($R_{y'z'}$) elliptical rings and displayed on *eye-charts*. Eye-folds associated with individual sheaths may thus be categorised by the R' value (where $R' = R_{yz}/R_{y'z'}$) into Type A or analogous-eye-folds ($R' = 1$), Type B or bulls-eye-folds ($R' > 1$) and Type C or cats-eye-folds ($R' < 1$).

(c) Sheath folds may contain greater elliptical ratios within the inner eye-shaped cross sections to define cats-eye-folds ($R' < 1$). Such patterns are consistently (>99%) associated with simple shear and general shear-dominated deformation.

(d) Sheath folds may contain lower elliptical ratios within the inner eye-shaped cross sections to define bulls-eye-folds ($R' > 1$). Such patterns are consistently (>90%) associated with constrictional deformation.

(e) More pronounced (R_{yz}) elliptical ratios are typically associated with sheath folds generated during general shear, although increasing shear strain (γ) and curvilinearity of the original periclinal fold hinge will also obviously increase R_{yz} during simple shear (Mies, 1993). If the relative component of pure shear (and therefore type of deformation) is uncertain, then ellipticity of eye-folds should not be used in isolation to determine shear strain (γ) (Lacassin and Mattauer, 1985).

(f) The ratio of layer thickness measured from sheath limbs to hinges (T_{yz}) displays a progressive increase from sheaths developed during constriction (T_{yz} 2.94), simple shear (T_{yz} 3.31) and general shear (T_{yz} 4.35) deformation.

(g) The correlation noted above between eye-fold patterns (R'), elliptical ratios (R_{yz}), and variations in layer thickness (T_{yz}) with the overall bulk strain regime in which the folds developed suggests that the type of deformation is the principal control governing the geometry of sheath folds. Although additional factors, such as pre-cursor folds locally originating parallel to subsequent shearing, may theoretically influence the geometry of resulting sheath folds, the overall correlation (>95%) of R' with strain type suggests that such influences are limited. These empirical relationships may thus allow sheath folds to act as both effective and robust discriminators of strain type.

(h) Future work will compare the data from sheath folds developed within metamorphic rocks with those formed in other deformational environments where intense ductile

shearing can occur, such as slumps, sub-glacial deformation zones, salt and magma flows.

Acknowledgements

Fieldwork for this paper was funded by the Edinburgh Geological Society and the Carnegie Trust, together with proceeds of the Lyell Fund of the Geological Society of London. We would like to thank the referees, Tim Bell, Nick Culshaw and Bernhard Grasemann together with the editor J. Hippertt, for careful and constructive reviews that have improved this manuscript.

Appendix. Data repository

Full listing of ~150 references for sheath fold data sources is provided in the online version of this article. This version can be found at 10.1016/j.jsg.2006.05.005.

References

Alsop, G.I., 1992. Progressive deformation and the rotation of contemporary fold axes in the Ballybofey Nappe, northwest Ireland. Geological Journal 27, 271–283.

Alsop, G.I., 1994. Relationships between distributed and localized shear in the tectonic evolution of a Caledonian fold and thrust zone, northwest Ireland. Geological Magazine 131, 123–136.

Alsop, G.I., Holdsworth, R.E., 1993. The distribution, geometry and kinematic significance of Caledonian buckle folds in the western Moine Nappe, northwestern Scotland. Geological Magazine 130, 353–362.

Alsop, G.I., Holdsworth, R.E., 1999. Vergence and facing patterns in large-scale sheath folds. Journal of Structural Geology 21, 1335–1349.

Alsop, G.I., Holdsworth, R.E., 2002. The geometry and kinematics of flow perturbation folds. Tectonophysics 350, 99–125.

Alsop, G.I., Holdsworth, R.E., 2004a. Shear zone folds: records of flow perturbation or structural inheritance? In: Alsop, G.I., Holdsworth, R.E., McCaffrey, K.J.W., Hand, M. (Eds.), Flow Processes in Faults and Shear Zones, Special Publications 224. Geological Society, London, pp. 177–199.

Alsop, G.I., Holdsworth, R.E., 2004b. The geometry and topology of natural sheath folds: a new tool for structural analysis. Journal of Structural Geology 26, 1561–1589.

Alsop, G.I., Holdsworth, R.E., 2004c. Shear zones – an introduction and overview. In: Alsop, G.I., Holdsworth, R.E., McCaffrey, K.J.W., Hand, M. (Eds.), Flow Processes in Faults and Shear Zones, Special Publications 224. Geological Society, London, pp. 1–9.

Alsop, G.I., Holdsworth, R.E., 2005. Discussion on evidence for non-plane strain flattening along the Moine thrust, Loch strath nan Aisinnin, northwest Scotland by Strine and Wojtal. Journal of Structural Geology 27, 781–784.

Alsop, G.I., Holdsworth, R.E. Flow perturbation folding in shear zones. In: Ries, A.C., Butler, R.W.H., Graham, R.D. (Eds.), Deformation of the Continental Crust: The legacy of Mike Coward. Special Publication of the Geological Society, London, in press.

Alsop, G.I., Holdsworth, R.E., Strachan, R.A., 1996. Transport-parallel cross folds within a mid-crustal Caledonian thrust stack, northern Scotland. Journal of Structural Geology 18, 783–790.

Azcarraga, J., Abalos, B., Gil Ibarguchi, J.I., 2002. On the relationship between kilometer-scale sheath folds, ductile thrusts and minor structures in the basal high-pressure units of the Cabo Ortegal complex (NW Spain). Journal of Structural Geology 24, 1971–1989.

Beunk, F.F., Page, L.M., 2001. Structural evolution of the accretional continental margin of the Paleoproterozoic Svecofennian orogen in southern Sweden. Tectonophysics 339, 67–92.

Boettcher, S.S., Mosher, S., 1998. Mid- to Late Cretaceous ductile deformation and thermal evolution of the crust in the northern Dome Rock Mountains, Arizona. Journal of Structural Geology 20, 745–764.

Boyle, A.P., 1987. A model for stratigraphic and structural inversions at Sulitjelma, central Scandes. Geological Magazine 124, 451–466.

Boyle, A.P., Dawes, I.P., 1991. Contrasted metamorphic and structural evolutions across a major ductile/brittle displacement zone in NW Connemara, western Ireland. Geologische Rundschau 80, 459–480.

Carey, S.W., 1962. Folding. Journal of the Alberta Society of Petroleum Geology 10, 95–144.

Carosi, R., Oggiano, G., 2002. Transpressional deformation in northwestern Sardinia (Italy): insights on the tectonic evolution of the Variscan Belt. Comptes Rendus Geoscience 334, 287–294.

Carreras, J., Estrada, A., White, S., 1977. The effects of folding on the *C*-axis fabrics of a quartz mylonite. Tectonophysics 39, 3–24.

Carreras, J., Druguet, E., Griera, A., 2005. Shear zone-related folds. Journal of Structural Geology 27, 1229–1251.

Chadwick, B., 1990. The stratigraphy of a sheet of supracrustal rocks within high-grade orthogneisses and its bearing on Late Archaean structure in southern West Greenland. Journal of the Geological Society, London 147, 639–652.

Cluzel, D., Jolivet, L., Cadet, J.P., 1991. Early Middle Paleozoic intraplate orogeny in the Ogcheon Belt (South Korea): a new insight on the Paleozoic buildup of East Asia. Tectonics 10, 1130–1151.

Cobbold, P.R., Quinquis, H., 1980. Development of sheath folds in shear regimes. Journal of Structural Geology 2, 119–126.

Coward, M.P., Potts, G.J., 1983. Complex strain patterns developed at the frontal and lateral tips to shear zones and thrust zones. Journal of Structural Geology 5, 383–399.

Crispini, L., Capponi, G., 1997. Quartz fabric and strain partitioning in sheath folds: an example from the Voltri group (Western Alps, Italy). Journal of Structural Geology 19, 1149–1157.

Culshaw, N., 2005. Buckle folding and deep-crustal shearing of high-grade gneisses at the junction of two major high-strain zones, central Gneiss Belt, Grenville Province, Ontario. Canadian Journal of Earth Sciences 42, 1907–1925.

Daigneault, R., St-Julien, P., Allard, G.O., 1990. Tectonic evolution of the northeast portion of the Archean Abitibi greenstone belt, Chibougamau area, Quebec. Canadian Journal of Earth Sciences 27, 1714–1736.

Dale, T.N., 1921. On concentric drag-folding in Alabama marble. American Journal of Science 2, 319–321.

Dalziel, I.W.D., Bailey, S.W., 1968. Deformed garnets in a mylonitic rock from the Grenville front and their tectonic significance. American Journal of Science 266, 542–562.

Dearman, W.R., 1969. Tergiversate folds from south-west England. Proceedings of the Ussher Society 2, 12–115.

D'el Rey Silva, L.J.H., Barros Neto, L.S., 2002. The Santa Terezinha-Campos Verdes emerald district, central Brazil: structural and Sm–Nd data to constrain the tectonic evolution of the neoproterozoic Brasilia belt. Journal of South American Earth Sciences 15, 693–708.

Diez Balda, M.A., Martinez Catalan, J.R., Ayarza Arribas, P., 1995. Syncollisional extensional collapse parallel to the orogenic trend in a domain of steep tectonics: the Salamanca Detachment zone (Central Iberian zone, Spain). Journal of Structural Geology 17, 163–182.

Dubey, A.K., Cobbold, P.R., 1977. Noncylindrical flexural slip folds in nature and experiment. Tectonophysics 38, 223–239.

Evans, J.P., Neves, D.S., 1992. Footwall deformation along Willard thrust, Sevier orogenic belt: implications for mechanisms, timing, and kinematics. Geological Society of America Bulletin 104, 516–527.

Ez, V., 2000. When shearing is a cause of folding. Earth Science Reviews 51, 155–172.

Faure, M., 1985. Microtectonic evidence for eastward ductile shear in the Jurassic orogen of SW Japan. Journal of Structural Geology 7, 175–186.

Fletcher, J.M., Bartley, J.M., 1994. Constrictional strain in a non-coaxial shear zone: implications for fold and rock fabric development, central Mojave

metamorphic core complex, California. Journal of Structural Geology 16, 555–570.

Forbes, C.J., Betts, P.G., Lister, G.S., 2004. Synchronous development of type 2 and type 3 fold interference patterns: evidence for recumbent sheath folds in the Allendale area, Broken hill, Australia. Journal of Structural Geology 26, 113–126.

Fossen, H., Holst, T.B., 1995. Northwest-verging folds and the northwestward movement of the Caledonian Jotun Nappe, Norway. Journal of Structural Geology 17, 3–15.

Fossen, H., Rykkelid, E., 1990. Shear zone structures in the Oygarden area, west Norway. Tectonophysics 174, 385–397.

Fowler, A.R., El Kalioubi, B., 2002. The Migif-Hafafit gneissis complex of the Egyptian Eastern Desert: fold interference patterns involving multiply deformed sheath folds. Tectonophysics 346, 247–275.

Gaudemer, Y., Tapponier, P., 1987. Ductile and brittle deformations in the northern Snake Range, Nevada. Journal of Structural Geology 9, 159–180.

Ghosh, S.K., 1993. Structural Geology: Fundamentals and Modern Developments. Pergamon Press, 598 pp.

Ghosh, S.K., Sengupta, S., 1984. Successive development of plane noncylindrical folds in progressive deformation. Journal of Structural Geology 6, 703–709.

Ghosh, S.K., Sengupta, S., 1987. Progressive development of structures in a ductile shear zone. Journal of Structural Geology 9, 277–287.

Ghosh, S.K., Khan, D., Sengupta, S., 1995. Interfering folds in constrictional deformation. Journal of Structural Geology 17, 1361–1373.

Ghosh, S.K., Hazra, S., Sengupta, S., 1999. Planar, non-planar and refolded sheath folds in the Phulad Shear Zone, Rajasthan, India. Journal of Structural Geology 21, 1715–1729.

Goscombe, B., 1991. Intense non-coaxial shear and the development of mega-scale sheath folds in the Arunta block, central Australia. Journal of Structural Geology 13, 299–318.

Grasemann, B., Wiesmayr, G., Draganits, E., Fusseis, F., 2004. Classification of Refold Structures. Journal of Geology 112, 119–125.

Hansen, E., 1971. Strain Facies. Springer-Verlag, New York, 207 pp.

Harms, T.A., Burger, H.R., Blednick, D.G., Cooper, J.M., King, J.T., Owen, D.R., Lowell, J., Sincock, M.J., Kranenburg, S.R., Pufall, A., Picornell, C.M., 2004. Character and origin of Precambrian fabrics and structures in the Tobacco Root Mountains, Montana. In: Brady, J.B., Burger, H.R., Cheney, J.T., Harms, T.A. (Eds.), Precambrian Geology of the Tobacco Root Mountains, Montana, Special Paper 377. Geological Society of America, pp. 203–226.

Henderson, J.R., 1981. Structural analysis of sheath folds with horizontal *X*-axes, northeast Canada. Journal of Structural Geology 3, 203–210.

Holdsworth, R.E., 1990. Progressive deformation structures associated with ductile thrusts in the Moine Nappe, Sutherland, N. Scotland. Journal of Structural Geology 12, 443–452.

Holdsworth, R.E., Roberts, A.M., 1984. Early curvilinear fold structures and strain in the Moine of the Glen Garry region, Inverness-shire. Journal of the Geological Society, London 141, 327–338.

Holdsworth, R.E., Strachan, R.A., Alsop, G.I., 2001. Geology of the Tongue District. Memoirs of the British Geological Survey, Sheet 114E (Scotland), 76 pp.

Jiang, D.Z., Williams, P.F., 1999. When do drag folds not develop into sheath folds in shear zones? Journal of Structural Geology 21, 577–583.

Kelly, N.M., Clarke, G.L., Carson, C.J., White, R.W., 2000. Thrusting in the lower crust: evidence from the Oygarden Islands, Kemp Land, East Antarctica. Geological Magazine 137, 219–234.

Klepeis, K.A., Crawford, M.L., Gehrels, G., 1998. Structural history of the crustal-scale coast shear zone north of Portland canal, southeast Alaska and British Columbia. Journal of Structural Geology 20, 883–904.

Koestler, A.G., 1988. Heterogeneous deformation and mylonitization of a granulite complex, Jotun–Valdres Nappe complex, central South Norway. Geological Journal 23, 1–13.

Kusky, T.M., Bradley, D.C., 1999. Kinematic analysis of mélange fabrics: examples and applications from the McHugh complex, Kenai peninsula, Alaska. Journal of Structural Geology 21, 1773–1796.

Lacassin, R., 1983. Microstructural evidence for a major ductile simple shear in the Monte-Rosa Nappe cover rocks. Comptes Rendus de l'Academie des Sciences 297, 613–618.

Lacassin, R., Mattauer, M., 1985. Kilometre-scale sheath fold at Mattmark and implications for transport direction in the Alps. Nature 315, 739–742.

Lefort, J.P., Aifa, T., Jelenska, M., Kadzialko-Hofmokl, M., Max, M.D., 2001. Paleomagnetic and AMS evidence for a Variscan ductile clockwise rotation of the Ile de Groix blueschists (south Brittany, France): consequence on the late Hercynian structural pattern of westernmost Europe. Tectonophysics 337, 223–235.

Lisle, R.J., 2003. Dupins indicatrix: a tool for quantifying periclinal folds on maps. Geological Magazine 140, 721–726.

Malavieille, J., 1987a. Kinematics of compressional and extensional ductile shearing deformation in a metamorphic core complex of the northeastern basin and range. Journal of Structural Geology 9, 541–554.

Malavieille, J., 1987b. Extensional shearing deformation and kilometer-scale ''a''-type folds in a cordilleran metamorphic core complex (Raft River Mountains, Northwestern Utah). Tectonics 6, 423–448.

Mattauer, M., Faure, M., Malavielle, J., 1981. Transverse lineation and large-scale structures related to Alpine obduction on Corsica. Journal of Structural Geology 3, 401–409.

Mawer, C.K., Williams, P.F., 1991. Progressive folding and foliation development in a sheared, coticule-bearing phyllite. Journal of Structural Geology 13, 539–555.

McCourt, S., Vearncombe, J.R., 1987. Shear zones bounding the central zone of the Limpopo Mobile belt, southern Africa. Journal of Structural Geology 9, 127–137.

Menardi-Noguera, A., 1988. Structural evolution of a Brianconnais cover nappe, the Caprauna-Armetta unit (Ligurian Alps, Italy). Journal of Structural Geology 10, 625–637.

Merschat, A.J., Hatcher, R.D., Davis, T.L., 2005. The northern Inner Piedmont, southern Appalachians, USA: kinematics of transpression and SW-directed mid-crustal flow. Journal of Structural Geology 27, 1252–1281.

Mies, J.W., 1993. Structural analysis of sheath folds in the Sylacauga marble group, Talladega slate belt, southern Appalachians. Journal of Structural Geology 15, 983–993.

Minigh, L.D., 1979. Structural analysis of sheath folds in a meta-chert from the western Italian Alps. Journal of Structural Geology 1, 275–282.

Mukhopadhyay, D., Matin, A., 1993. The structural anatomy of the Sandur schist belt – a greenstone belt in the Dharwar craton of South India. Journal of Structural Geology 15, 309–322.

Mukhopadhyay, D., Sengupta, S., 1979. ''Eyed folds'' in Precambrian marbles from southeastern Rajasthan, India. Geological Society of America Bulletin 90, 397–404.

Mvondo, H., den Brok, S.W.J., Mvondo Ondoa, J., 2003. Evidence for symmetric extension and exhumation of the Yaounde nappe (Pan-African belt, Cameroon). Journal of African Earth Sciences 36, 215–231.

Nicholson, R., 1963. Eyed folds and interference patterns in the Sokumfjell Marble Group, Northern Norway. Geological Magazine 100, 59–68.

Nicholson, R., Walton, B.J., 1963. The structural geology of the Navervatin-Storglomvatn area, Glomfjord, Northern Norway. Saertrykk av Norsk Geologisk Tidsskrift 43, 1–58.

Oliver, G.J.H., 1994. Mid-crustal detachment and domes in the central zone of the Damaran orogen, Namibia. Journal of African Earth Sciences 19, 331–344.

Passchier, C.W., Trouw, R.A.J., 2005. Microtectonics, second ed. Springer-Verlag, Berlin/Heidelberg, 366 pp.

Patrick, B.E., 1988. Synmetamorphic structural evolution of the Seward Peninsula blueschist terrane, Alaska. Journal of Structural Geology 10, 555–565.

Platt, J.P., 1983. Progressive refolding in ductile shear zones. Journal of Structural Geology 5, 619–622.

Poli, L.C., Oliver, G.J.H., 2001. Constrictional deformation in the Central Zone of the Damaran Orogen, Namibia. Journal of African Earth Sciences 33, 303–321.

Puelles, P., Mulchrone, K.F., Abalos, B., Gil Ibarguchi, J.I., 2005. Structural analysis of high-pressure shear zones (Bacariza formation, Cabo Ortegal, NW Spain). Journal of Structural Geology 27, 1046–1060.

Quinquis, H., Audren, C., Brun, J.P., Cobbold, P., 1978. Intensive progressive shear in Ile de Groix blueschists and compatibility with subduction or obduction. Nature 274, 43–45.

Ramsay, J.G., 1962. Interference patterns produced by the superposition of folds of similar type. Journal of Geology 70, 466–481.

Ramsay, J.G., 1980. Shear zone geometry: a review. Journal of Structural Geology 2, 83–99.

Ramsay, J.G., Huber, M.I., 1987. The techniques of modern structural geology. In: Folds and Fractures, vol. 2. Academic Press.

Salinas-Prieto, J.C., Monod, O., Faure, M., 2000. Ductile deformations of opposite vergence in the eastern part of the Guerrero terrane (SW Mexico). Journal of South American Earth Sciences 13, 389–402.

Schmid, S., Casey, M., 1986. Complete fabric analysis of some commonly observed quartz *c*-axis patterns. Mineral and Rock Deformation: Laboratory Studies – The Paterson Volume. Geophysical Monograph 36. American Geophysical Union, pp. 263–286.

Schulmann, K., Melka, R., Lobkowicz, M.Z., Ledru, P., Lardeaux, J.M., Autran, A., 1994. Contrasting styles of deformation during progressive nappe stacking at the southeastern margin of the Bohemian Massif (Thaya Dome). Journal of Structural Geology 16, 355–370.

Searle, M.P., Warren, C.J., Waters, D.J., Parrish, R.R., 2004. Structural evolution, metamorphism and restoration of the Arabian continental margin, Saih Hatat region, Oman Mountains. Journal of Structural Geology 26, 451–473.

Sengupta, S., Ghosh, S.K., 2004. Analysis of transpressional deformation from geometrical evolution of mesoscopic structures from Phulad shear zone, Rajasthan, India. Journal of Structural Geology 26, 1961–1976.

Seno, S., Dallagiovanna, G., Vanossi, M., 1998. From finite strain data to strain history: a model for a sector of the Ligurian Alps, Italy. Journal of Structural Geology 20, 573–585.

Skjernaa, L., 1989. Tubular folds and sheath folds: definitions and conceptual models for their development, with examples from the Grapesvare area, northern Sweden. Journal of Structural Geology 11, 689–703.

Srivastava, D.C., 2001. Deformation pattern in the Precambrian basement around Masuda, central Rajasthan. Journal of the Geological Society of India 57, 197–222.

Stauffer, M.R., Lewry, J.F., 1993. Regional setting and kinematic features of the Needel Falls Shear Zone, Trans-Hudson Orogen. Canadian Journal of Earth Sciences 30, 1338–1354.

Tabor, J.R., Hudleston, P.J., 1991. Deformation in an Archean subprovince boundary, northern Minnesota. Canadian Journal of Earth Sciences 28, 292–307.

Terry, M.P., Robinson, P., 2003. Evolution of amphibolite-facies structural features and boundary conditions for deformation during exhumation of high- and ultrahigh-pressure rocks. Nordoyane, Western Gneiss region, Norway. Tectonics 22. TC001349.

Teyssier, C., Amri, C., Hobbs, B.E., 1988. South Arunta block: the internal zones of a Proterozoic overthrust in Central Australia. Precambrian Research 40, 157–173.

Vassllo, J.J., Wilson, C.J.L., 2002. Palaeoproterozoic regional-scale non-coaxial deformation: an example from eastern Eyre peninsula, South Australia. Journal of Structural Geology 24, 1–24.

Veenhof, R.P., Stel, H., 1991. A cleavage triple point and it's meso-scopic structures: the Mustio Sink (Svecofennides of SW Finland). Precambrian Research 50, 269–282.

Voll, G., 1960. New work on petrofabrics. Liverpool and Manchester Geological Journal 2, 503–567.

Vollmer, F.W., 1988. A computer model of sheath-nappes formed during crustal shear in the Western Gneiss Region, central Norwegian Caledonides. Journal of Structural Geology 10, 735–743.

White, J.C., Flagler, P.A., 1992. Deformation within part of a major crustal shear zone, Parry Sound, Ontario: structure and kinematics. Canadian Journal of Earth Sciences 29, 129–141.

Williams, P.F., Zwart, H.J., 1977. A model for the development of the Seve-Koli Caledonian nappe complex. In: Saxena, S.K., Bhattacharji, S. (Eds.), Energetics of Geological Processes. Springer-Verlag, New York, pp. 169–187.

Yassaghi, A., James, P.R., Flottmann, T., 2000. Geometric and kinematic evolution of asymmetric ductile shear zones in thrust sheets, southern Adelaide Fold-Thrust Belt, South Australia. Journal of Structural Geology 22, 889–912.